Journal of Computational Physics (2019)

SAND2019-14970J

Contents lists available at ScienceDirect

Journal of Computational Physics

journal homepage: www.elsevier.com/locate/jcp

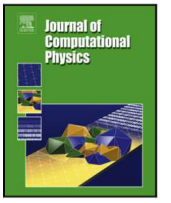

Stability analysis and discretization of A-Φ time domain integral equations for multiscale electromagnetics

Thomas E. Roth[a,b], Weng C. Chew[b,c,*]

[a] *Sandia National Laboratories, Albuquerque, NM, USA*
[b] *Department of Electrical and Computer Engineering, University of Illinois at Urbana-Champaign, Urbana, IL, USA*
[c] *School of Electrical and Computer Engineering, Purdue University, West Lafayette, IN, USA*

ARTICLE INFO

Article history:
Received 22 Jul 2018
Accepted 4 Nov 2019
Available online 9 Nov 2019

Keywords: Electromagnetics, Time domain integral equations, Stability analysis

ABSTRACT

The growth of applications at the intersection between electromagnetic and quantum physics is necessitating the creation of novel computational electromagnetic solvers. This work presents a new set of time domain integral equations (TDIEs) formulated directly in terms of the magnetic vector and electric scalar potentials that can be used to meet many of the requirements of this emerging area. Stability for this new set of TDIEs is achieved by leveraging an existing rigorous functional framework that can be used to determine suitable discretization approaches to yield stable results in practice. The basics of this functional framework are reviewed before it is shown in detail how it may be applied in developing the TDIEs of this work. Numerical results are presented which validate the claims of stability and accuracy of this method over a wide range of frequencies where traditional methods would fail.

1. Introduction

The rapid improvements in quantum theory is continually resulting in a diverse range of technological advances. For many applications, classical and quantum electromagnetic theory already have, and will continue to play a key role in the creation of novel technologies that leverage these improvements [1, 2]. This includes development in areas obviously related to electromagnetics, such as quantum optics and atom-photon interactions [1, 3, 4]. However, electromagnetic theory is also necessary in less obvious applications; for instance, those requiring Casimir force or near-field heat transfer calculations [2, 5, 6]. For each application area, suitable computational electromagnetic solvers are needed to bridge the gap between analytically solvable systems and those desired to be numerically analyzed for problems of practical interest.

*Corresponding author.
e-mail: wcchew@purdue.edu (Weng C. Chew)

Sandia National Laboratories is a multimission laboratory managed and operated by National Technology & Engineering Solutions of Sandia, LLC, a wholly owned subsidiary of Honeywell International Inc., for the U.S. Department of Energy's National Nuclear Security Administration under contract DE-NA0003525.

However, the diverse set of applications imposes a similarly diverse set of requirements for computational electromagnetic solvers to be widely applicable. One common and challenging requirement is to have deeply multiscale solvers; i.e., an accurate and efficient solution can be found over a wide range of length scales with respect to the wavelength of the electromagnetic radiation [1]. Different applications also require different physical quantities to be calculated. For instance, in the interaction of a charged particle and an electromagnetic field, the magnetic vector potential ($\mathbf{A}$) and the electric scalar potential (Φ) are needed in the solution of the Schrödinger equation [7]. Other examples include: the Maxwell stress tensor in Casimir force calculations; and dyadic Green's functions for atom-photon interactions or stimulated emission rate calculations [1, 8, 9, 10].

To address the growing needs of these and other applications, the $\mathbf{A}$-Φ formulation has been developed [1]. This formulates the computational electromagnetic solvers directly in terms of the vector and scalar potentials, leading to equations that perform well from very long to short wavelengths. This is a unique and novel property of the equations, which is not typically realized in their discretized counterparts based directly on the electric ($\mathbf{E}$) and magnetic ($\mathbf{H}$) fields [11, 12, 13]. Additionally, the $\mathbf{A}$-Φ formulation has the benefit of typically being more easily integrated into quantum physics calculations, where these quantities are deemed more fundamental than $\mathbf{E}$ and $\mathbf{H}$ [1, 2, 7]. These properties make computational electromagnetic solvers developed from the $\mathbf{A}$-Φ formulation ideal candidates for meeting the needs of emerging applications that rely on quantum physics.

Past work has extended the $\mathbf{A}$-Φ formulation to the following methods: finite-difference time-domain [7], frequency domain finite element method [14], and frequency domain integral equations [15]. The focus of this work is to continue this development by extending the $\mathbf{A}$-Φ formulation to time domain integral equations (TDIEs). This process was begun in [16], which presented two sets of $\mathbf{A}$-Φ TDIEs and demonstrated their numerical stability and favorable performance in extracting results at low frequencies. The current work supports [16] by presenting the rigorous functional analysis that was essential in successfully deriving and implementing the $\mathbf{A}$-Φ TDIEs of [16].

The interest in TDIEs stems from the fact that they combine the many benefits of time domain methods with those of integral equations. For instance, time domain methods can perform broadband simulations and can be applied to nonlinear problems. Integral equations automatically satisfy the radiation condition and allow for flexible geometric modeling that only requires surface discretizations, greatly reducing the number of unknowns compared to differential equation based methods. With the development of fast algorithms, TDIEs may also be applied to unprecedentedly large problems that would be prohibitive for other methods [17, 18]. Combining these benefits of TDIEs with the other properties of the $\mathbf{A}$-Φ formulation leads to a numerical solver that can be used in many of the mentioned applications.

Although there is promise in using TDIEs, they are no panacea. A prevalent issue with TDIEs has been a history of instability when using a traditional marching-on-in-time (MOT) discretization scheme [19]. This has attempted to be overcome or avoided in a number of ways; e.g., using filtering/averaging schemes [20], bandlimited interpolation functions [21], or convolution quadrature techniques [22]. However, these approaches have not been widely adopted due to impacts on accuracy or efficiency of the methods. Instead, most focus has remained on MOT methods, and after decades of work the key factors needed to achieve stable TDIE systems in practice have been largely determined. The two most important factors are the accurate numerical evaluation of the relevant space-time integrals and the basis and testing functions used to find a matrix representation of the integral operator. Accurate numerical integrations have been addressed by a number of methods, e.g. [23, 24, 25], which are directly applicable to $\mathbf{A}$-Φ TDIEs. Only the particular method used in this work will be discussed, although the other methods are certainly viable as well.

Selection of appropriate basis and testing functions is a more subtle requirement. Basis functions should be selected from the domain of the integral operator, while testing functions should come from the dual space to the range of the operator [26, 27]. If these functions are not selected appropriately, the practical stability of the TDIE can be substantially compromised. As a result, it is imperative to determine the Sobolev spaces that act as the domain and range (so its dual may be easily found) for different integral operators so that they may be discretized appropriately.

Unfortunately, determining the relevant Sobolev spaces for a TDIE is not a simple task. Progress in this field is mostly confined to French mathematical literature [28, 29]; however, some more accessible works also exist [19, 27, 30, 31]. In particular, [27, 31] review the Sobolev spaces for the electric field integral equation (EFIE) developed in [28], and then demonstrate how the functional analysis can be extended to cover the differentiated EFIE.

In this work, we aim to apply these previously developed functional analysis methods to develop $\mathbf{A}$-Φ formulation TDIEs. In an effort to make this development understandable by the widest audience possible, this work reviews many key points that have often been scattered in the literature. For those readers that do not require this review, we have outlined the key portions of the manuscript below so that they may navigate this work quickly.

- Section 2: Reviews the functional framework from its simplest fundamental concepts to make it more accessible

to a wider audience. For those already familiar with this framework, the key portions are (27), (29), and Variational Problem 2, which define much of the relevant notation used in this work.

- Section 3: The frequency domain **A**-Φ integral equations are briefly reviewed before using the functional framework of Section 2 to justify the derivation of appropriate **A**-Φ TDIEs. The two sets of **A**-Φ TDIEs are summarized in Variational Problems 4 and 5, with stability bounds developed in Section 3.4.
- Section 4: Presents the detailed discretization of the **A**-Φ TDIEs, where Section 4.2 discusses the key concepts for determining correct basis and testing functions for the TDIEs based on the presented variational problems.
- Section 5: Numerical results are presented that validate all claims of instability or stability of the various formulations and discretizations discussed. Results demonstrating the accuracy and low frequency performance of the **A**-Φ TDIEs are also shown.

2. Background

Before presenting the details of the functional framework that will be utilized throughout this work, we briefly review the general type of equations of interest to this work. In particular, the time domain EFIE will be reviewed, which acts as the starting point for deriving **A**-Φ TDIEs later in this work.

To begin formulating the time domain EFIE, consider a time-varying electric field incident upon a scatterer embedded in a homogeneous background medium defined by permeability μ, permittivity ϵ, and speed of light c. As initial conditions, it is assumed that the incident field, denoted by $\mathbf{E}^{\text{inc}}$, has not yet reached the scatterer defined by a surface S, for all $t < 0$. If the scatterer is a perfect electric conductor (PEC), enforcing the boundary condition that the total tangential electric field on S is 0 yields the traditional EFIE [11]:

$$\hat{n}\times\Big(\int_S\Big[\mu\frac{\dot{\mathbf{J}}(\mathbf{r}',\tau)}{4\pi R}-\nabla\int_{-\infty}^{\tau}\frac{\nabla'\cdot\mathbf{J}(\mathbf{r}',t')}{4\pi R\epsilon}dt'\Big]dS'\times\hat{n}\Big)=\hat{n}\times(\mathbf{E}^{\text{inc}}(\mathbf{r},t)\times\hat{n}),\tag{1}$$

where $\hat{n}$ is the outward pointing unit normal vector to the surface S at location $\mathbf{r}$, $R = |\mathbf{r}-\mathbf{r}'|$, $\tau = t - R/c$ is the retarded time, and a dot above a quantity denotes a temporal derivative with respect to t. In (1), $\mathbf{J} = \hat{n}'\times\mathbf{H}$ is the equivalent surface current density induced on S that produces the appropriate scattered field, $\mathbf{E}^{\text{sc}}$, such that the total field is given by $\mathbf{E}^{\text{inc}} + \mathbf{E}^{\text{sc}}$.

This TDIE has been studied extensively in the past, with particular emphasis placed on determining discretization schemes that are stable, accurate, and efficient. Although there is a substantial amount of literature on this subject, the particular works of interest are related to the development of a rigorous functional framework used to analyze TDIEs and determine stable discretization schemes. This was begun in the seminal work of [32] which analyzed acoustic TDIEs, before being extended to 2D electromagnetic systems in [33]. Analysis of 3D electromagnetic systems was performed in [28], which also performed a thorough analysis of the Sobolev spaces necessary to analyze electromagnetic TDIEs that many later works have been based upon. Note that although we only focus on the analysis from these works, alternative approaches to rigorously study TDIEs have also been devised [34].

It is this functional framework that is adopted in this work to develop stable **A**-Φ TDIEs. As such, it is the focus of this section to introduce the necessary background concepts so that this functional framework may be understood by as broad an audience as possible. Toward this end, in Section 2.1, we give the simple, intuitive reasons for introducing Sobolev spaces, and discuss a basic example in the frequency domain. Following this, the relevant spatial Sobolev spaces for solving integral equations are discussed. With the necessary foundations in place, Section 2.2 discusses the full functional framework for TDIEs that will be used in this work. Finally, with all the necessary tools in place, the EFIE is revisited within the context of the functional framework in Section 2.3.

The mathematical results discussed in this section are heavily drawn from [19, 27, 29, 35], and do not constitute new work. However, there is novelty in the presentation of the material in as simplified a manner as possible to allow it to be understood by the widest audience possible. Further, it brings many concepts together into one piece of work that were previously scattered between different areas of the literature (and in different languages).

2.1. Sobolev Space Background

In physics, Sobolev spaces are used to rigorously define the needed properties of functions so that they can be considered to be "physical" solutions to differential or integral equations. The particular property that is desired is

that the solution produces finite energy within a domain [35]. This typically takes the form of requiring the function and some number of derivatives to be square integrable, i.e., members of the Hilbert space L^2. This can be easily seen by considering that the total electromagnetic energy in a volume V is given by

$$\begin{aligned}\tilde{\mathcal{E}}(\omega) &= \frac{1}{2}\int_V \left(\epsilon|\tilde{\mathbf{E}}(\mathbf{r},\omega)|^2 + \mu|\tilde{\mathbf{H}}(\mathbf{r},\omega)|^2\right)dV \\ &= \frac{1}{2}\int_V \left(\epsilon|\tilde{\mathbf{E}}(\mathbf{r},\omega)|^2 + \frac{1}{\mu|\omega|^2}|\nabla\times\tilde{\mathbf{E}}(\mathbf{r},\omega)|^2\right)dV,\end{aligned} \tag{2}$$

for the time-harmonic case, with angular frequency defined by ω and a tilde used to denote that a quantity is in the frequency domain. For the remainder of this paper, the explicit dependence on ω for frequency domain functions will often be omitted for brevity when it is clear from context. Note that in the frequency domain, all quantities will in general be complex numbers, while time domain quantities will be real. As a result, the inner products and norms in the frequency and time domains are defined in the traditional manner to reflect this.

From (2), it can be seen that for $\tilde{\mathcal{E}}$ to be finite requires that both $\tilde{\mathbf{E}}$ and $\nabla\times\tilde{\mathbf{E}}$ be in L^2 (or equivalently, in terms of $\tilde{\mathbf{H}}$). As a result, when trying to define function spaces for which solutions to differential or integral equations should be sought in, it is necessary to consider Sobolev spaces.

For the example given here, the Sobolev space would be defined as

$$H(\text{curl},\omega,V) \coloneqq \left\{\tilde{\mathbf{v}} : \tilde{\mathbf{v}} \in L^2(V)^3, \nabla\times\tilde{\mathbf{v}} \in L^2(V)^3, \|\tilde{\mathbf{v}}\|_{H(\text{curl},\omega,V)} < \infty\right\}, \tag{3}$$

$$\|\tilde{\mathbf{v}}\|_{H(\text{curl},\omega,V)} \coloneqq \left(\|\tilde{\mathbf{v}}\|^2 + \frac{1}{|\omega|^2}\|\nabla\times\tilde{\mathbf{v}}\|^2\right)^{\frac{1}{2}}, \tag{4}$$

and $\|\cdot\|$ is the standard L^2 norm over V. The additional ω scaling factor in (4) is included to make the norm more closely match the calculation of electromagnetic energy given in (2), which will be crucial in the later results. As a result, if a function is in $H(\text{curl},\omega,V)$ it can be concluded that it has finite electromagnetic energy, as desired.

A related space can also be defined that will be found to be useful. This is

$$H(\text{div},\omega,V) \coloneqq \left\{\tilde{\mathbf{v}} : \tilde{\mathbf{v}} \in L^2(V)^3, \nabla\cdot\tilde{\mathbf{v}} \in L^2(V), \|\tilde{\mathbf{v}}\|_{H(\text{div},\omega,V)} < \infty\right\}, \tag{5}$$

$$\|\tilde{\mathbf{v}}\|_{H(\text{div},\omega,V)} \coloneqq \left(\|\tilde{\mathbf{v}}\|^2 + \frac{1}{|\omega|^2}\|\nabla\cdot\tilde{\mathbf{v}}\|^2\right)^{\frac{1}{2}}. \tag{6}$$

A similar Sobolev space that is related to the energy of scalar wave functions can also be defined. This space is

$$H^1(\omega,V) \coloneqq \left\{\tilde{u} : \tilde{u} \in L^2(V), \nabla\tilde{u} \in L^2(V)^3, \|\tilde{u}\|_{H^1(\omega,V)} < \infty\right\}, \tag{7}$$

$$\|\tilde{u}\|_{H^1(\omega,V)} \coloneqq \left(|\omega|^2\|\tilde{u}\|^2 + \|\nabla\tilde{u}\|^2\right)^{\frac{1}{2}}. \tag{8}$$

This can be related to the energy of a wave function $\tilde{u}$ in V [19]. This can be intuitively seen by recognizing that the first term in (8) acts like a kinetic energy and the second term acts like a potential energy. Typically for analysis purely in the frequency domain the scaling of these norms by ω in (4) and (8) is largely unimportant. However, it will be critical when attempting to derive properties in the time domain, as will be seen later.

Up to this point, the Sobolev spaces discussed were defined over a volume for simplicity. However, since we are concerned with solving surface integral equations, such as that in (1), we need to consider the definitions of Sobolev spaces that contain the boundary values of the functions in V (i.e., spaces defined on a 2D surface in a 3D space). Since the bounding surface (denoted as S) of the volume has a measure of zero, the exact mathematical definition of these boundary values becomes complicated. This is similar, in principle, to the problem of specifying the value of an L^2-"function" at a point. To address this problem, the *trace theorems*[1] were developed. The result of these theorems is a definition of trace operators that make rigorous the meaning of restricting a function from Sobolev spaces defined

over V to ones defined over S.

Before continuing with the definition of relevant surface Sobolev spaces, it should be noted that the mathematical analysis typically done is for closed surfaces. However, a number of surface integral equations are applicable to open surfaces, such as the EFIE. Similarly, the **A**-Φ TDIEs developed in this work can also be applied to open surfaces without any difficulty.

With respect to typical Sobolev spaces used in physics, the trace operators lead to the definitions of two new spaces, $H^{\frac{1}{2}}(S)$ and its dual space $H^{-\frac{1}{2}}(S)$, which are introduced in a simple manner in [35]. The space $H^{\frac{1}{2}}(S)$ consists of boundary values of functions in $H^1(V)$, while $H^{-\frac{1}{2}}(S)$ consists of the normal derivatives of functions in $H^1(V)$. The norms for these spaces are related to a form of Hölder continuity, which is necessary to make the most severe singularities encountered in solving integral equations be integrable. For the purpose of this work, it will be more useful to have ω-scaled versions of these norms to connect to the time domain, resulting in the spaces $H^{\frac{1}{2}}(\omega, S)$ and $H^{-\frac{1}{2}}(\omega, S)$ which are defined in [19]. The norms for these spaces are more easily defined using a more abstract approach utilizing the Fourier transform of functions on S. Due to the overly technical nature of the definition of these spaces and that the norms will not need to be explicitly used, they will not be reproduced here. The interested reader is referred to [19] for more details.

As will be seen throughout this work, $H^{-\frac{1}{2}}(\omega, S)$ will be used more frequently as it is important for defining part of the Sobolev spaces that are typically relevant for solving electromagnetic integral equations [29]. The two spaces are

$$H^{-\frac{1}{2}}(\mathrm{div}, \omega, S) \coloneqq \left\{ \tilde{\mathbf{v}} : \tilde{\mathbf{v}} \in H^{-\frac{1}{2}}(\omega, S)^3, \hat{n} \cdot \tilde{\mathbf{v}} = 0, \nabla \cdot \tilde{\mathbf{v}} \in H^{-\frac{1}{2}}(\omega, S) \right\} \tag{9}$$

and

$$H^{-\frac{1}{2}}(\mathrm{curl}, \omega, S) \coloneqq \left\{ \tilde{\mathbf{v}} : \tilde{\mathbf{v}} \in H^{-\frac{1}{2}}(\omega, S)^3, \hat{n} \cdot \tilde{\mathbf{v}} = 0, \nabla \times \tilde{\mathbf{v}} \in H^{-\frac{1}{2}}(\omega, S)^3 \right\}. \tag{10}$$

Note that the divergence in (9) and the curl in (10) are to be interpreted as surface divergences and curls [29, 35]. The norms associated with these spaces are

$$\|\tilde{\mathbf{v}}\|_{H^{-\frac{1}{2}}(\mathrm{div},\omega,S)} \coloneqq \left(\|\tilde{\mathbf{v}}\|^2_{H^{-\frac{1}{2}}(\omega,S)} + \frac{1}{|\omega|^2} \|\nabla \cdot \tilde{\mathbf{v}}\|^2_{H^{-\frac{1}{2}}(\omega,S)} \right)^{\frac{1}{2}} \tag{11}$$

and

$$\|\tilde{\mathbf{v}}\|_{H^{-\frac{1}{2}}(\mathrm{curl},\omega,S)} \coloneqq \left(\|\tilde{\mathbf{v}}\|^2_{H^{-\frac{1}{2}}(\omega,S)} + \frac{1}{|\omega|^2} \|\nabla \times \tilde{\mathbf{v}}\|^2_{H^{-\frac{1}{2}}(\omega,S)} \right)^{\frac{1}{2}}. \tag{12}$$

It is also important to note that these spaces are dual spaces to each other, and that if $\tilde{\mathbf{v}} \in H^{-\frac{1}{2}}(\mathrm{div}, \omega, S)$ then $\hat{n} \times \tilde{\mathbf{v}} \in H^{-\frac{1}{2}}(\mathrm{curl}, \omega, S)$ (and vice-versa) [29, 35]. In the engineering literature, these two spaces are typically referred to as the spaces of div-conforming and curl-conforming functions defined on a surface S, respectively. An example of a function in $H^{-\frac{1}{2}}(\mathrm{div}, \omega, S)$ is the Rao-Wilton-Glisson (RWG) function, which is commonly used in the engineering literature to discretize surface integral equations [27, 36]. As stated above, this also means that $\hat{n} \times$RWG is in $H^{-\frac{1}{2}}(\mathrm{curl}, \omega, S)$.

With the needed surface Sobolev spaces defined, it is instructive to consider an example of how they are connected through trace operators to some of the previously defined volume Sobolev spaces. Taking the example of $H(\mathrm{curl}, \omega, V)$, a possible trace operator would be $\hat{n} \times \tilde{\mathbf{v}}|_S$ for $\tilde{\mathbf{v}} \in H(\mathrm{curl}, \omega, V)$, which would produce a function in $H^{-\frac{1}{2}}(\mathrm{div}, \omega, S)$ [29, 35]. An important property of any trace operator is that it is a bounded operator. For the example above, we have

$$\|\hat{n} \times \tilde{\mathbf{v}}\|_{H^{-\frac{1}{2}}(\mathrm{div},\omega,S)} \leq C(V) |\omega|^{\frac{1}{2}} \|\tilde{\mathbf{v}}\|_{H(\mathrm{curl},\omega,V)}, \tag{13}$$

where $C(V)$ is a constant that only depends on V [29]. Although mathematically useful, these operators also have

[1] Note that in this context the use of the word *trace* is unrelated to other common traces used in physics, such as that of a matrix or an operator.

physical meaning. For instance, in integral equations in electromagnetics, the equivalent electric and magnetic current densities are typically used as unknown source functions, defined as $\tilde{\mathbf{J}} = \hat{n}\times\tilde{\mathbf{H}}$ and $\tilde{\mathbf{M}} = \tilde{\mathbf{E}}\times\hat{n}$, respectively [37]. When these definitions are considered in the context of (13), it illustrates the physically clear boundedness of the equivalent current densities by the electromagnetic energy in some surrounding volume.

Combining many of the concepts discussed in this section, it is possible to establish bounds on the results of applying different integral operators to functions in appropriate Sobolev spaces. As a particular example, we consider the integral operator from the EFIE for perfectly conducting objects embedded in a homogeneous background medium, which is

$$\mathcal{L}\{\tilde{\mathbf{J}}\}(\mathbf{r},\omega) \coloneqq \int_S \left[i\omega\mu\tilde{g}(\mathbf{r},\mathbf{r}')\tilde{\mathbf{J}}(\mathbf{r}') - \frac{1}{i\omega\epsilon}\nabla\tilde{g}(\mathbf{r},\mathbf{r}')\nabla'\cdot\tilde{\mathbf{J}}(\mathbf{r}')\right]dS'. \tag{14}$$

In (14),

$$\tilde{g}(\mathbf{r},\mathbf{r}') = \frac{e^{ikR}}{4\pi R} \tag{15}$$

is the free-space Green's function with $k = \omega/c$ and $\omega = \gamma + i\sigma$ and $\sigma > 0$ [29]. The need for ω to be defined in this way will be made more clear in Section 2.2. Note that the notation $\mathcal{L}\{\tilde{\mathbf{J}}\}(\mathbf{r},\omega)$ is used to stress that this is being viewed as a function defined by the $\mathcal{L}$ operator being applied to the function $\tilde{\mathbf{J}}$. In particular, $\mathcal{L}\{\tilde{\mathbf{J}}\}(\mathbf{r},\omega)$ can be identified as the scattered electric field produced by $\tilde{\mathbf{J}}$.

For $\tilde{\mathbf{J}} \in H^{-\frac{1}{2}}(\text{div},\omega,S)$ and Ω being some external (unbounded or bounded) region to S, the following bound can be established:

$$\|\mathcal{L}\{\tilde{\mathbf{J}}(\cdot,\omega)\}\|_{H(\text{curl},\omega,\Omega)} \leq C(S,\sigma)|\omega|^{\frac{1}{2}}\,\|\tilde{\mathbf{J}}(\cdot,\omega)\|_{H^{-\frac{1}{2}}(\text{div},\omega,S)}. \tag{16}$$

This is established in two basic steps. The first step involves applying a trace operator to bound the energy of the scattered electric field in Ω by a norm taken only over the surface. In particular, we make use of (11) in [29], which is

$$\|\mathcal{L}\{\tilde{\mathbf{J}}(\cdot,\omega)\}\|_{H(\text{curl},\omega,\Omega)} \leq C(S)|\omega|^{-\frac{1}{2}}\|\hat{n}\times\mathcal{L}\{\tilde{\mathbf{J}}(\cdot,\omega)\}\|_{H^{-\frac{1}{2}}(\text{div},\omega,S)}. \tag{17}$$

At this point, properties of the integral representations being used to solve the physical problem can be exploited to derive bounds on the scattered energy by the source function that produced it. For this example, this type of bound is given in (16) of [29], which is

$$\|\hat{n}\times\mathcal{L}\{\tilde{\mathbf{J}}(\cdot,\omega)\}\|_{H^{-\frac{1}{2}}(\text{div},\omega,S)} \leq C(S,\sigma)|\omega|\|\tilde{\mathbf{J}}(\cdot,\omega)\|_{H^{-\frac{1}{2}}(\text{div},\omega,S)}. \tag{18}$$

More details related to the derivation of this type of bound relevant to acoustic integral equations is given in [19]. At this point, (17) and (18) can be combined to give (16), which demonstrates that the energy of the scattered electric field is bounded by the source that produced it. Although this is physically obvious, it will be seen in the following sections that bounds like (16) play a much more pivotal role than establishing these obvious properties. In particular, the ω-dependence of these bounds will be instrumental in determining appropriate Sobolev spaces for TDIE problems.

2.2. Extension to the Time Domain

To begin the process of determining the Sobolev spaces relevant to TDIEs, it will be useful to again consider the electromagnetic energy. Converting (2) to the time domain gives

$$\mathcal{E}(t) = \frac{1}{2}\int_V \left(\epsilon|\mathbf{E}(\mathbf{r},t)|^2 + \mu^{-1}|\int_{-\infty}^{t}\nabla\times\mathbf{E}(\mathbf{r},t')dt'|^2\right)dV. \tag{19}$$

Following the frequency domain example, we define the following Sobolev space to capture the needed properties for a function to have finite electromagnetic energy. This space is

$$H(\text{curl},t,V) \coloneqq \left\{\mathbf{v} : \mathbf{v}\in L^2(V)^3, \nabla\times\mathbf{v}\in L^2(V)^3, \|\mathbf{v}(\cdot,t)\|_{H(\text{curl},t,V)} < \infty\right\} \tag{20}$$

with norm

$$\|\mathbf{v}(\cdot,t)\|_{H(\mathrm{curl},t,V)} \coloneqq \left(\|\mathbf{v}(\cdot,t)\|^2 + \| \int_{-\infty}^{t} \nabla\times\mathbf{v}(\cdot,t')dt'\|^2\right)^{\frac{1}{2}}. \tag{21}$$

Note that this norm is computing the energy at a fixed instant in time.

For a function to be a valid solution to a TDIE, it will need to produce finite energy according to the norm in (21) at all instants in time. Considering this, it will be a very difficult task to define the necessary properties of functions to be useful solutions to TDIEs directly in the time domain. Instead, the approach advocated in [19] is to derive properties in the Laplace domain and then transform these back to the time domain (this is also the approach in [27, 28, 29]). The general process is the following. Since the functions for the problems considered are assumed to be zero $\forall t < 0$, the Fourier-Laplace transform yields analytic functions whose convergence toward zero at infinity can be given through a Paley-Wiener theorem. By invoking Parseval's theorem, the convergence of the appropriate integral over the Laplace domain can be used to bound the time domain results.

Before considering a concrete example, we first need to set our notation related to the Fourier-Laplace transform. We will consider the space of Laplace transformable functions from Hilbert space E to be defined as

$$LT(\sigma,E) \coloneqq \left\{f : e^{-\sigma t}f \in L^1(\mathbb{R}_+,E), \sigma > 0\right\}, \tag{22}$$

where $\mathbb{R}_+$ is used to denote that the time domain functions are only defined for $t>0$. In this work, E will be taken to be one of the spatial Sobolev spaces defined earlier. Then, the Fourier-Laplace transform can be given as

$$\tilde{f}(\mathbf{r},\omega) = \int_{-\infty}^{\infty} f(\mathbf{r},t)e^{i\omega t}dt, \tag{23}$$

where $\omega = \gamma + i\sigma$. Within this context, Parseval's theorem becomes

$$\int_{-\infty}^{\infty} e^{-2\sigma t}\|f(\cdot,t)\|_E^2\, dt = \frac{1}{2\pi}\int_{-\infty+i\sigma}^{\infty+i\sigma} \|\tilde{f}(\cdot,\omega)\|_E^2\, d\omega, \tag{24}$$

which as alluded to earlier will allow a connection between the time and frequency domain analysis [19].

As a concrete example of the process for determining the Sobolev space that solutions to a TDIE should be found in, let us consider the integral operator from the EFIE in the time domain. This is denoted as $\mathcal{L}\{\mathbf{J}\}(\mathbf{r},t)$, and is defined so that the left-hand side of (1) is $\hat{n}\times(\mathcal{L}\{\mathbf{J}\}(\mathbf{r},t)\times\hat{n})$. As previously mentioned, it is difficult to directly determine what properties will be needed of $\mathbf{J}$ so that the function $\mathcal{L}\{\mathbf{J}\}(\mathbf{r},t)$ (i.e., the scattered electric field) will have finite energy for all time. However, by applying Parseval's theorem, we have

$$\int_{-\infty}^{\infty} e^{-2\sigma t}\|\mathcal{L}\{\mathbf{J}\}(\cdot,t)\|_{H(\mathrm{curl},t,\Omega)}^2\, dt = \frac{1}{2\pi}\int_{-\infty+i\sigma}^{\infty+i\sigma} \|\mathcal{L}\{\tilde{\mathbf{J}}\}(\cdot,\omega)\|_{H(\mathrm{curl},\omega,\Omega)}^2\, d\omega. \tag{25}$$

Using the bound in (16) then gives

$$\int_{-\infty}^{\infty} e^{-2\sigma t}\|\mathcal{L}\{\mathbf{J}\}(\cdot,t)\|_{H(\mathrm{curl},t,\Omega)}^2\, dt \leq C(S,\sigma)\frac{1}{2\pi}\int_{-\infty+i\sigma}^{\infty+i\sigma} |\omega|\, \|\tilde{\mathbf{J}}(\cdot,\omega)\|_{H^{-\frac{1}{2}}(\mathrm{div},\omega,S)}^2\, d\omega. \tag{26}$$

From this, we can directly see the needed properties of $\tilde{\mathbf{J}}$ so that the scattered electric field will remain finite for all time. Note that this only establishes the minimum properties that will be needed of a function to be considered as a possible solution to the integral equation. In particular, this bound *does not* prove the stability of the integral equation. To do this, we will need to determine a bound on $\tilde{\mathbf{J}}$ in terms of the incident field (which from (26) also then bounds the scattered field).

With the result of (26), we may now define a set of *ad hoc* Sobolev spaces developed in [28] that will be used for

the functional framework for TDIEs. The first family of spaces are for vector functions, and are given as

$$\begin{aligned}\mathscr{H}_{\text{div}}^{s_1,s_2} &:= H_\sigma^{s_1}(\mathbb{R}_+, H^{s_2}(\text{div}, \omega, S)) \\ &:= \left\{ \mathbf{f}(\mathbf{r},t) \in LT\Big(\sigma, H^{s_2}(\text{div}, \omega, S)\Big), \|\mathbf{f}\|^2_{\mathscr{H}_{\text{div}}^{s_1,s_2}} < \infty \right\}\end{aligned} \tag{27}$$

where

$$\|\mathbf{f}\|^2_{\mathscr{H}_{\text{div}}^{s_1,s_2}} := \frac{1}{2\pi} \int_{-\infty+i\sigma}^{\infty+i\sigma} |\omega|^{2s_1} \|\tilde{\mathbf{f}}(\cdot,\omega)\|^2_{H^{s_2}(\text{div},\omega,S)} d\omega. \tag{28}$$

From (28), it is understood that s_1 is related to the temporal differentiability of the functions, while s_2 is related to the spatial differentiability. Another useful set of spaces can also be defined by replacing div for curl in (27) and (28). Importantly, the norm for this space can be related back to the electromagnetic energy, as seen in (26), so that it will be useful in establishing the stability properties of TDIEs [27, 28].

With the first set of Sobolev spaces defined, we can see how they are used by continuing with the concrete example of the EFIE. It is seen by comparing (26) to the families of Sobolev spaces defined in (27) that $\mathbf{J}(\mathbf{r},t)$ should be a member of $\mathscr{H}_{\text{div}}^{\frac{1}{2},-\frac{1}{2}}$.

In addition to the vector Sobolev spaces just discussed, we also need a similar set of spaces for scalar functions. In particular, we define

$$\begin{aligned}\mathcal{H}^{s_1,s_2} &:= H_\sigma^{s_1}(\mathbb{R}_+, H^{s_2}(\omega, S)) \\ &:= \left\{ f(\mathbf{r},t) \in LT\Big(\sigma, H^{s_2}(\omega, S)\Big), \|f\|^2_{\mathcal{H}^{s_1,s_2}} < \infty \right\}\end{aligned} \tag{29}$$

where

$$\|f\|^2_{\mathcal{H}^{s_1,s_2}} := \frac{1}{2\pi} \int_{-\infty+i\sigma}^{\infty+i\sigma} |\omega|^{2s_1} \|\tilde{f}(\cdot,\omega)\|^2_{H^{s_2}(\omega,S)} d\omega. \tag{30}$$

In order to test the different integral equations to form their matrix representations, we will make use of space-time pairings. A pairing takes an element of a function space and an element of the dual function space and returns a number from the field that the function spaces are defined over. This is the correct way to discretize integral equations, since testing functions should be selected from the dual space to the range of the integral operator [26, 27]. The first pairing that will be used is defined for vector functions, and is

$$\langle \mathbf{f}, \mathbf{g} \rangle_\sigma := \int_{-\infty}^{\infty} e^{-2\sigma t} \int_S \mathbf{f}(\mathbf{r},t) \cdot \mathbf{g}(\mathbf{r},t) dS\, dt, \tag{31}$$

for $\mathbf{f} \in \mathscr{H}_{\text{div}}^{-s_1,s_2}$ and $\mathbf{g} \in \mathscr{H}_{\text{curl}}^{s_1,s_2}$. The second pairing is for scalar functions, and is

$$\langle f, g \rangle_\sigma := \int_{-\infty}^{\infty} e^{-2\sigma t} \int_S f(\mathbf{r},t) g(\mathbf{r},t) dS\, dt, \tag{32}$$

for $f \in \mathcal{H}^{-s_1,-s_2}$ and $g \in \mathcal{H}^{s_1,s_2}$. The structure of these pairing will be useful for quickly determining the range space of various integral operators later.

To aid in understanding, Table 1 lists sample functions for spatial Sobolev spaces, while Table 2 lists functions for temporal Sobolev spaces. These example functions cover most of the spaces that basis or testing functions will need to be selected from throughout this work.

2.3. EFIE Variational Formulation

With the necessary Sobolev spaces introduced, the EFIE may now be considered within this functional framework. Before we can express the variational problem for the EFIE, we need to determine what function space $\mathbf{E}^{\text{inc}}$ should be

Table 1: Example Functions For Spatial Sobolev Spaces

Sobolev Space	**Sample Function**
$H^{-\frac{1}{2}}(\text{div}, \omega, S)$	RWG [36]
$H^{-\frac{1}{2}}(\omega, S)$	Pulse/Constant

Table 2: Example Functions For Temporal Sobolev Spaces

Sobolev Space	**Sample Function**
$H_\sigma^{-\frac{3}{2}}(\mathbb{R}_+, \cdot)$	Dirac delta
$H_\sigma^{-\frac{1}{2}}(\mathbb{R}_+, \cdot)$	Rectangle
$H_\sigma^{\frac{1}{2}}(\mathbb{R}_+, \cdot)$	Triangle
$H_\sigma^{\frac{3}{2}}(\mathbb{R}_+, \cdot)$	Quadratic B-spline [27]

contained in. To determine this Sobolev space we make use of the following bound implied in [27] and [38]. This is

$$\|\tilde{\mathbf{J}}(\cdot,\omega)\|_{H^{-\frac{1}{2}}(\text{div},\omega,S)} \leq C(S,\sigma)\,|\omega|\,\|\tilde{\mathbf{E}}^{\text{inc}}(\cdot,\omega)\times\hat{n}\|_{H^{-\frac{1}{2}}(\text{div},\omega,S)}, \tag{33}$$

which is established by considering the relationship between the integral equations and the corresponding partial differential equations that they relate to [19]. More details on deriving this type of bound can be found in [19] for acoustic integral equations. Recalling the discussion about the trace operator in (13), we see that these bounds demonstrate that the source function for the EFIE will be bounded by the incident electromagnetic energy. This is the last piece needed to demonstrate the stability of the TDIE.

To show this, we recall that the electromagnetic energy radiated by $\mathbf{J}$ for all time was related to the frequency domain using Parseval's theorem in (25). This was combined with (16) to bound the electromagnetic energy by the norm of the source function, as shown in (26). This established the need for $\mathbf{J} \in \mathscr{H}_{\text{div}}^{\frac{1}{2},-\frac{1}{2}}$. By now using the bound in (33), we see that

$$\int_{-\infty}^{\infty} e^{-2\sigma t}\|\mathcal{L}\{\mathbf{J}\}(\cdot,t)\|^2_{H(\text{curl},t,\Omega)}\,dt \leq C(S,\sigma)\frac{1}{2\pi}\int_{-\infty+i\sigma}^{\infty+i\sigma}|\omega|^3\,\|\tilde{\mathbf{E}}^{\text{inc}}(\cdot,\omega)\times\hat{n}\|^2_{H^{-\frac{1}{2}}(\text{div},\omega,S)}\,d\omega. \tag{34}$$

This demonstrates the need for $(\mathbf{E}^{\text{inc}}\times\hat{n})$ to at least be in $\mathscr{H}_{\text{div}}^{\frac{3}{2},-\frac{1}{2}}$ for the problem to be well-posed. This then establishes the desired stability property, since (34) shows that the scattered electromagnetic energy will be bounded by the incident electromagnetic energy (which will always be finite for physical problems).

To summarize, the major components of the logical chain used to establish the stability of the TDIE can be broken into the following steps.

1. Determine how the scattered electromagnetic energy in the time domain can be related to the energy in the frequency domain, e.g., in (25).
2. Use properties of the integral operator to bound the scattered energy by the norm of the source function that produced the scattered field, demonstrated in (16).
3. Bound the norm of the source function by the energy of the incident field, e.g., in (33).

It is important to remember from earlier discussions that these norms, although complicated, are meaningful since they can all be related back to the electromagnetic energy.

With all the appropriate Sobolev spaces now determined, it is possible to express the EFIE in terms of an appropriate variational problem, for which a number of theorems have already been established [27].

Variational Problem 1. *(Electric Field Integral Equation)*
$\forall(\mathbf{E}^{\text{inc}}\times\hat{n}) \in \mathscr{H}_{\text{div}}^{\frac{3}{2},-\frac{1}{2}}$ *search for* $\mathbf{J} \in \mathscr{H}_{\text{div}}^{\frac{1}{2},-\frac{1}{2}}$ *such that* $\forall\mathbf{J}' \in \mathscr{H}_{\text{div}}^{\frac{1}{2},-\frac{1}{2}}$:

$$\left\langle \ddot{\mathbf{J}}'(\mathbf{r},t), \int_S \left[\mu\frac{\dot{\mathbf{J}}(\mathbf{r}',\tau)}{4\pi R} - \nabla\int_{-\infty}^{\tau}\frac{\nabla'\cdot\mathbf{J}(\mathbf{r}',t')}{4\pi R\epsilon}dt'\right]dS'\right\rangle_\sigma = \left\langle \ddot{\mathbf{J}}'(\mathbf{r},t), \hat{n}\times(\mathbf{E}^{\text{inc}}(\mathbf{r},t)\times\hat{n})\right\rangle_\sigma . \tag{35}$$

In this variational problem, $\mathbf{J}'$ is to be considered as the testing function. It should be noted, however, that $\ddot{\mathbf{J}}'$ is what is actually used in the equation (and would therefore enter into the discretization approach). The reason for the variational problem being written in this way is stylistic, i.e., having the main basis and testing Sobolev spaces be the same. This notation is adopted throughout this work to minimize the modifications made to equations taken from the literature in this work.

Considering the definition of $\mathbf{E}^{\text{inc}}(\mathbf{r},t)\times\hat{n}$, it is seen that $\ddot{\mathbf{J}}'$ is a member of the appropriate dual space for this integral equation to be well-tested. Further, this also helps in providing an easy way to determine the range of the integral operator. This will prove to be especially useful in Sections 3 and 4 when we consider integral equations that have not been previously analyzed like the EFIE has.

An important property of this variational problem is that the existence and uniqueness of the solution to an equivalent variational problem were established in [28]. Further, the stability of the solution to the equivalent variational problem has also been proven [28]. The stability of the TDIE is concisely given in terms of a bound on $\mathbf{J}$, i.e.,

$$\|\mathbf{J}\|_{\mathscr{H}_{\text{div}}^{\frac{1}{2},-\frac{1}{2}}} \leq C(S,\sigma)\|\mathbf{E}^{\text{inc}}\times\hat{n}\|_{\mathscr{H}_{\text{div}}^{\frac{3}{2},-\frac{1}{2}}}, \tag{36}$$

which is equivalent to (33). This can be seen by explicitly writing out the norms in (36) using the definition given in (28). Through equations like (34), the stability of the overall TDIE is seen. It will be shown later in Section 4 how information from variational problems like this one can be used to determine stable discretization strategies for a variety of TDIEs.

Before moving on to developing **A**-Φ TDIEs, it will be useful to consider a slightly different form of the EFIE. In particular, the current continuity equation is used to introduce the charge density, denoted as ρ. From [27], it can be concluded that $\rho \in \mathcal{H}^{\frac{1}{2},-\frac{1}{2}}$. Making these changes (see [27] for details), we arrive at the equivalent variational problem that was analyzed in [28].

Variational Problem 2. *(Double-Source Electric Field Integral Equation)*
$\forall(\mathbf{E}^{\text{inc}}\times\hat{n}) \in \mathscr{H}_{\text{div}}^{\frac{3}{2},-\frac{1}{2}}$ *search for* $(\rho,\mathbf{J}) \in \mathcal{H}^{\frac{1}{2},-\frac{1}{2}} \times \mathscr{H}_{\text{div}}^{\frac{1}{2},-\frac{1}{2}}$ *such that* $\forall\mathbf{J}' \in \mathscr{H}_{\text{div}}^{\frac{1}{2},-\frac{1}{2}}$:

$$\left\langle \ddot{\mathbf{J}}'(\mathbf{r},t), \int_S \left[\mu\frac{\dot{\mathbf{J}}(\mathbf{r}',\tau)}{4\pi R} + \nabla\frac{\rho(\mathbf{r}',\tau)}{4\pi R\epsilon}\right]dS'\right\rangle_\sigma = \left\langle \ddot{\mathbf{J}}'(\mathbf{r},t), \hat{n}\times(\mathbf{E}^{\text{inc}}(\mathbf{r},t)\times\hat{n})\right\rangle_\sigma . \tag{37}$$

This variational problem serves as a better starting point for deriving **A**-Φ TDIEs. Since this is the more useful form of the EFIE for this work, we will refer to (37) as the EFIE for the remainder of this work. Similar to Variational Problem 1, the existence, uniqueness, and stability of this variational problem have been established [28]. In fact, these properties for Variational Problem 1 are actually inherited from the proofs of them for Variational Problem 2 [27]. In addition to the stability bound given in (36), there also is a bound on ρ, which is

$$\|\rho\|_{\mathcal{H}^{\frac{1}{2},-\frac{1}{2}}} \leq C(S,\sigma)\|\mathbf{E}^{\text{inc}}\times\hat{n}\|_{\mathscr{H}_{\text{div}}^{\frac{3}{2},-\frac{1}{2}}}. \tag{38}$$

At this point, the essential details of the functional framework developed by various mathematicians to analyze electromagnetic TDIEs have been introduced. It is believed that the step-by-step introduction of this material presented here without the complicated proofs should help a wider audience understand the intuitive aspects of this functional framework. With this background in place, we now begin to develop appropriate **A**-Φ TDIEs.

3. A-Φ TDIEs

Before presenting the methodology for deriving stable **A**-Φ TDIEs, we briefly develop the frequency domain integral equations of [15] in Section 3.1. Following this, **A**-Φ TDIEs that can be stably discretized are derived

in Sections 3.2 and 3.3. The results of this derivation are two different **A**-Φ variational problems which can be stably discretized. To complete the mathematical details of this formulation, Section 3.4 shows how the necessary bounds can be determined to prove the stability of the two sets of TDIEs that were derived. Finally, in Section 3.5, a variational problem for the **A**-Φ formulation discussed in Section 3.1 is presented. This aids in outlining how no MOT discretization scheme will lead to stable results in the time domain for this formulation. The details of discretizing these variational problems are deferred until Section 4, and numerical results validating all claims of stability or instability are presented in Section 5.

3.1. A-Φ Formulation Background

To begin developing the **A**-Φ frequency domain integral equations of [15], we introduce the potentials in the standard way so that Maxwell's equations are automatically satisfied. In particular,

$$\tilde{\mathbf{B}} = \nabla \times \tilde{\mathbf{A}}, \tag{39}$$

$$\tilde{\mathbf{E}} = i\omega\tilde{\mathbf{A}} - \nabla\tilde{\Phi}, \tag{40}$$

and $\tilde{\mathbf{B}} = \mu\tilde{\mathbf{H}}$. To derive decoupled wave equations for $\tilde{\mathbf{A}}$ and $\tilde{\Phi}$ the Lorenz gauge is selected, i.e., $\nabla \cdot \tilde{\mathbf{A}} = i\omega\mu\epsilon\tilde{\Phi}$. The resulting wave equations are

$$\nabla^2\tilde{\mathbf{A}} + k^2\tilde{\mathbf{A}} = -\mu\tilde{\mathbf{J}} \tag{41}$$

$$\nabla^2\tilde{\Phi} + k^2\tilde{\Phi} = -\tilde{\rho}/\epsilon. \tag{42}$$

We seek to derive surface integral equations that when solved produce solutions to these two wave equations simultaneously. One approach to do this is to leverage Green's theorems to first derive decoupled surface integral equations appropriate to each wave equation [37]. This process for (42) is very standard (e.g., see [37, 39]), but has only recently been performed for (41), with substantial details presented in [1]. Once the decoupled integral equations have been derived, they can later be coupled together by enforcing the appropriate gauge conditions.

Alternatively, the approach of [15] can be followed. This begins by starting with the decoupled integral equation derived in [1] that solves (41) and enforcing the Lorenz gauge. The resulting integral equation when considering scattering from a PEC object defined by surface S embedded in a homogeneous medium characterized by ϵ and μ is

$$\int_S \left[\mu\tilde{g}(\mathbf{r},\mathbf{r}')\tilde{\mathbf{J}}(\mathbf{r}') + \nabla'\tilde{g}(\mathbf{r},\mathbf{r}')\tilde{\Sigma}(\mathbf{r}')\right] dS' = -\tilde{\mathbf{A}}^{\text{inc}}(\mathbf{r}), \tag{43}$$

where $\tilde{\Sigma} = \hat{n}' \cdot \tilde{\mathbf{A}}$, which along with $\tilde{\mathbf{J}}$ are the unknowns of the equation. Before determining another equation to produce a solvable system, it is worthwhile to consider the physical meaning of $\tilde{\Sigma}$. This can be seen by considering the definition of an equivalent surface charge density, i.e.,

$$\tilde{\rho}(\mathbf{r}') = \hat{n}' \cdot (\epsilon\tilde{\mathbf{E}}(\mathbf{r}')) = i\omega\epsilon\tilde{\Sigma}(\mathbf{r}') - \epsilon\hat{n}' \cdot \nabla'\tilde{\Phi}(\mathbf{r}'). \tag{44}$$

It is then seen that the physical importance of $\tilde{\Sigma}$ is that it acts as a contribution to the surface charge density.

To arrive at a solvable system, an additional equation is still needed. One possible equation to complete the system can be found by taking the divergence of (43) and applying the Lorenz gauge condition [15]. This gives

$$\int_S \left[\tilde{g}(\mathbf{r},\mathbf{r}')\nabla' \cdot \tilde{\mathbf{J}}(\mathbf{r}') + \omega^2\epsilon\tilde{g}(\mathbf{r},\mathbf{r}')\tilde{\Sigma}(\mathbf{r}')\right] dS' = -i\omega\epsilon\tilde{\Phi}^{\text{inc}}(\mathbf{r}), \tag{45}$$

which can be shown to be equivalent to enforcing the standard integral equation that solves (42) for a PEC surface [37]. It is important to note that the application of the Lorenz gauge was essential to the derivation of this system, since it takes otherwise independent solutions of (41) and (42) and ties them together so that the solutions represent electromagnetic potentials, as desired [40]. As a result, the scattered potentials produced by the solutions to (43) and (45) will be able to be combined to produce unique electromagnetic fields, but will themselves only be able to be considered unique up to appropriately defined gauge functions.

It is also important to note that (43) and (45) may be combined to yield the EFIE [15]. As a result, it will be possible to perform a derivation of appropriate **A**-Φ integral equations by starting at the EFIE and deriving back to a

more fundamental representation similar to (43) and (45). This is the approach that will be taken in the next section.

Although this system can be made to be equivalent to the EFIE, solving (43) and (45) together leads to a system that has vastly superior performance to the EFIE at low frequencies. The physically intuitive reason for this is that as the frequency lowers, (43) captures the quasi-magnetostatic physics while (45) captures the quasi-electrostatic physics. This is demonstrated in [15] where a variety of different numerical examples are presented, validating this formulation in the frequency domain. This is in contrast to the EFIE, which mixes the scalar and vector potential contributions to the scattered fields into a single equation. The imbalance between these contributing terms in the EFIE then leads to the well-known low frequency breakdown [11]. Another interpretation is that the EFIE only uses two of Maxwell's equations in its derivation. As the frequency lowers, these two equations begin to decouple, which manifests itself as the low frequency breakdown of the EFIE. In contrast, the **A**-Φ formulation utilizes all four of Maxwell's equations. As a result, as the frequency lowers, the natural decoupling of the electric and magnetic fields is able to still be properly captured.

In addition to the favorable low frequency performance, the **A**-Φ formulation discussed in this section also performs better for dense meshes than the EFIE [15]. Further, the matrix system for this formulation can be identified as a saddle point problem [41]. This means that a constraint preconditioner may be utilized, greatly improving the performance of this formulation when iterative solvers must be used. Preconditioners are also beneficial in the time domain, where an iterative solution to a matrix system is needed during each time step of the simulation [12]. This is particularly so for low frequency or multiscale problems where the system matrix to be solved can be dense. Importantly, this same type of preconditioner has been shown to be effective in the time domain in [42], and will be able to be formed for the TDIEs derived in this work. Combining this with the favorable low frequency properties of these TDIEs makes them applicable to analyzing multiscale geometries. A further benefit is that constraint preconditioners have a simple form and can be efficiently formed [15]. This is in contrast to other preconditioning methods that have been suggested for the EFIE, namely Calderón preconditioners, which although very successful, are more time consuming to construct and implement in code than a constraint preconditioner [12].

Unfortunately, when (43) and (45) are converted to the time domain, the resulting system is highly unstable numerically in the form of highly oscillatory and ever-increasing solutions. A rigorous functional analysis can show that these two equations cannot be discretized together to yield a stable system. This will be demonstrated in Sections 4 and 5, after the appropriate functional analysis for **A**-Φ TDIEs has been presented. Since there are no choices of basis and testing functions that will result in a stable MOT system, alternative equations that can be stably discretized together must be derived. The major portion of this derivation is done in Section 3.2, with the remainder of the derivation and a summary of the final variational problems in Section 3.3.

3.2. Preliminary Derivation

The approach used to derive **A**-Φ TDIEs in this section is in principle similar to that of [27], where it was shown how the stability results of the EFIE could be extended to also cover the differentiated EFIE within the same functional framework. Since the EFIE is derivable from the **A**-Φ system (see [15]), it will be possible to extend the functional framework for the EFIE to the **A**-Φ equations. This will be done by starting with the EFIE and then deriving corresponding **A**-Φ TDIEs from it. From this, it will be possible to determine the appropriate spaces for the **A**-Φ TDIEs by monitoring how the various Sobolev spaces change throughout the derivation. This is much simpler than attempting to perform the functional analysis directly on the **A**-Φ system, and further aids in the process by providing useful physical insight into an otherwise unfamiliar problem.

From the discussion in Section 3.1, it is clear that the EFIE needs to be separated into two equations to determine corresponding **A**-Φ integral equations. To begin doing this, the surface charge density and incident electric field are rewritten in terms of the vector and scalar potentials, given by

$$\rho(\mathbf{r}', t) = -\epsilon[\Pi(\mathbf{r}', t) + \hat{n}' \cdot \nabla' \Phi(\mathbf{r}', t)] \tag{46}$$

and

$$\mathbf{E}^{\text{inc}}(\mathbf{r}, t) \times \hat{n} = -[\dot{\mathbf{A}}^{\text{inc}}(\mathbf{r}, t) + \nabla \Phi^{\text{inc}}(\mathbf{r}, t)] \times \hat{n}, \tag{47}$$

where $\Pi = \hat{n}' \cdot \dot{\mathbf{A}}$. Note that as long as $\mathbf{E}^{\text{inc}}$ is a solution to Maxwell's equations this decomposition can always be done. However, care is needed in determining correct forms for $\mathbf{A}^{\text{inc}}$ and Φ^{inc} to solve a desired problem. Examples for common types of excitations are given in [15].

Using (46) and (47), the EFIE given in (37) can be written as

$$\left\langle \ddot{\mathbf{J}}'(\mathbf{r},t), \mathcal{L}_{\partial_t \mathrm{V}}\{\mathbf{J},\Pi\}(\mathbf{r},t) - \nabla \mathcal{L}_{\mathrm{H}}\{\hat{n}'\cdot\nabla'\Phi\}(\mathbf{r},t)\right\rangle_{\sigma} = \left\langle \ddot{\mathbf{J}}'(\mathbf{r},t), -\hat{n}\times([\dot{\mathbf{A}}^{\mathrm{inc}}(\mathbf{r},t) + \nabla\Phi^{\mathrm{inc}}(\mathbf{r},t)]\times\hat{n})\right\rangle_{\sigma}, \tag{48}$$

where

$$\mathcal{L}_{\partial_t \mathrm{V}}\{\mathbf{J},\Pi\}(\mathbf{r},t) = \int_S \left[\mu\frac{\dot{\mathbf{J}}(\mathbf{r}',\tau)}{4\pi R} - \nabla\frac{\Pi(\mathbf{r}',\tau)}{4\pi R}\right] dS' \tag{49}$$

and

$$\mathcal{L}_{\mathrm{H}}\{\hat{n}'\cdot\nabla'\Phi\}(\mathbf{r},t) = \int_S \frac{\hat{n}'\cdot\nabla'\Phi(\mathbf{r}',\tau)}{4\pi R} dS'. \tag{50}$$

For brevity, the dependence of the functions in the space-time pairings on $\mathbf{r}$ and t will be omitted for the remainder of this work.

Before (48) can be separated into two equations, it is important to consider the Sobolev spaces of the introduced functions. From Variational Problem 2, it is already known that $\rho \in \mathcal{H}^{\frac{1}{2},-\frac{1}{2}}$ and that $(\mathbf{E}^{\mathrm{inc}}\times\hat{n}) \in \mathscr{H}_{\mathrm{div}}^{\frac{3}{2},-\frac{1}{2}}$. For (46) and (47) to be meaningful then requires that the sums in each equation is a member of the appropriate function space. In (46), this can be guaranteed by requiring that Π and $\hat{n}'\cdot\nabla'\Phi$ be members of $\mathcal{H}^{\frac{1}{2},-\frac{1}{2}}$. Similarly, (47) can be made meaningful by requiring $(\dot{\mathbf{A}}^{\mathrm{inc}}\times\hat{n})$ and $(\nabla\Phi^{\mathrm{inc}}\times\hat{n})$ to be in $\mathscr{H}_{\mathrm{div}}^{\frac{3}{2},-\frac{1}{2}}$. It should be noted that this is the simplest way to conclude what Sobolev spaces would be appropriate for the introduced potentials. By more rigorously considering the properties of the partial differential equations they satisfy, the same conclusions can be reached.

By selecting the Sobolev spaces in this way, it is now possible to separate (48) into two equations. To begin, the linearity of the pairings is used to give

$$\left\langle \ddot{\mathbf{J}}', \mathcal{L}_{\partial_t \mathrm{V}}\{\mathbf{J},\Pi\}\right\rangle_{\sigma} - \left\langle \ddot{\mathbf{J}}', \nabla\mathcal{L}_{\mathrm{H}}\{\hat{n}'\cdot\nabla'\Phi\}\right\rangle_{\sigma} = -\left\langle \ddot{\mathbf{J}}', \hat{n}\times(\dot{\mathbf{A}}^{\mathrm{inc}}\times\hat{n})\right\rangle_{\sigma} - \left\langle \ddot{\mathbf{J}}', \hat{n}\times(\nabla\Phi^{\mathrm{inc}}\times\hat{n})\right\rangle_{\sigma}. \tag{51}$$

It is important to note that because of the choices of Sobolev spaces discussed in the last paragraph, each of the pairings in (51) yields a finite value individually, allowing the linearity of the pairing to be used.

Now, Gauss' theorem may be used to rewrite the second and fourth pairings to transfer the gradient operator to the testing functions, yielding

$$\left\langle \ddot{\mathbf{J}}', \mathcal{L}_{\partial_t \mathrm{V}}\{\mathbf{J},\Pi\}\right\rangle_{\sigma} + \left\langle \nabla\cdot\ddot{\mathbf{J}}', \mathcal{L}_{\mathrm{H}}\{\hat{n}'\cdot\nabla'\Phi\}\right\rangle_{\sigma} = -\left\langle \ddot{\mathbf{J}}', \hat{n}\times(\dot{\mathbf{A}}^{\mathrm{inc}}\times\hat{n})\right\rangle_{\sigma} + \left\langle \nabla\cdot\ddot{\mathbf{J}}', \Phi^{\mathrm{inc}}\right\rangle_{\sigma}. \tag{52}$$

By noting that the second and fourth pairings in (52) constitute the scalar Huygens' principle, it can be concluded that they are equal to one another [37]. This allows (52) to be separated by physical arguments into

$$\left\langle \ddot{\mathbf{J}}', \mathcal{L}_{\partial_t \mathrm{V}}\{\mathbf{J},\Pi\}\right\rangle_{\sigma} = -\left\langle \ddot{\mathbf{J}}', \hat{n}\times(\dot{\mathbf{A}}^{\mathrm{inc}}\times\hat{n})\right\rangle_{\sigma} \tag{53}$$

$$\left\langle \nabla\cdot\ddot{\mathbf{J}}', \mathcal{L}_{\mathrm{H}}\{\hat{n}'\cdot\nabla'\Phi\}\right\rangle_{\sigma} = \left\langle \nabla\cdot\ddot{\mathbf{J}}', \Phi^{\mathrm{inc}}\right\rangle_{\sigma}. \tag{54}$$

Although the EFIE has been successfully separated into two equations, (53) and (54) do not constitute a solvable system. This is because there are two equations, but three unknowns: namely $\mathbf{J}$, Π, and $\hat{n}'\cdot\nabla'\Phi$. However, it is possible to rewrite (54) so that it uses the same unknowns as (53). This is done by noting that the continuity equation with ρ rewritten in terms of the potentials given in (46) is

$$\int_{-\infty}^{t} \epsilon^{-1}\nabla'\cdot\mathbf{J}(\mathbf{r}',t')dt' = \Pi(\mathbf{r}',t) + \hat{n}'\cdot\nabla'\Phi(\mathbf{r}',t). \tag{55}$$

Substituting this into (54) for $\hat{n}'\cdot\nabla'\Phi$ then gives

$$\left\langle \nabla\cdot\ddot{\mathbf{J}}', \mathcal{L}_{\mathrm{S}}\{\mathbf{J},\Pi\}\right\rangle_{\sigma} = \left\langle \nabla\cdot\ddot{\mathbf{J}}', \Phi^{\mathrm{inc}}\right\rangle_{\sigma}, \tag{56}$$

where

$$\mathcal{L}_{\mathrm{S}}\{\mathbf{J},\Pi\}(\mathbf{r},t)=\int_S\Big[\int_{-\infty}^{\tau}\frac{\nabla'\cdot\mathbf{J}(\mathbf{r}',t')}{4\pi R\epsilon}dt'-\frac{\Pi(\mathbf{r}',\tau)}{4\pi R}\Big]dS'. \tag{57}$$

Although (53) and (56) could be solved together, it would produce both a nonsymmetric MOT matrix system (e.g., the equivalent of the matrix defined in (101) but for the equations just mentioned), and more importantly, an unstable system. The reason for instability is similar to that of a system based on time domain versions of (43) and (45) and will be discussed in Section 3.3, while the remainder of this section will focus on beginning to make the discretized matrix system symmetric (and simultaneously able to be stably discretized).

To begin moving toward a symmetric system, we first note that the primary reason the system will not be symmetric is because of testing (56) with $\nabla\cdot\ddot{\mathbf{J}}'$. That is, taking the divergence of functions typically used to represent current densities will make the system nonsymmetric. However, it is possible to rewrite this testing process by noting that $\mathbf{J}'$ should behave like an electric current density to be a good testing function. An intuitive way to understand this is by noting that the Rumsey reaction theorem provides a physically motivated way to determine appropriate testing functions for different numerical methods [43, 44]. Since the integral operator in (57) produces a component of the electric field, the reaction theorem suggests that this equation should be tested with an electric current density. This also aligns with the Sobolev space properties already stated for $\mathbf{J}'$. Additionally, for $\mathbf{J}'$ to truly act like an electric current density it should satisfy a continuity equation, as required in [27]. By rewriting $\nabla\cdot\ddot{\mathbf{J}}'$ using the continuity equation, (56) becomes

$$\langle\dddot{\rho}',\mathcal{L}_{\mathrm{S}}\{\mathbf{J},\Pi\}\rangle_\sigma=\left\langle\dddot{\rho}',\Phi^{\mathrm{inc}}\right\rangle_\sigma, \tag{58}$$

where ρ' is a testing function that has characteristics similar to a charge density. Using a testing function that behaves like a charge density, rather than taking the divergence of a function representing a current density, will allow a symmetric matrix system to be achieved, as will be seen in Section 4.

The developments of this section are summarized in the following variational problem.

Variational Problem 3.
$\forall(\dot{\mathbf{A}}^{\mathrm{inc}}\times\hat{n})\in\mathscr{H}_{\mathrm{div}}^{\frac{3}{2},-\frac{1}{2}}$ *and* $\forall\Phi^{\mathrm{inc}}\in\mathcal{H}^{\frac{5}{2},\frac{1}{2}}$ *search for* $(\Pi,\mathbf{J})\in\mathcal{H}^{\frac{1}{2},-\frac{1}{2}}\times\mathscr{H}_{\mathrm{div}}^{\frac{1}{2},-\frac{1}{2}}$ *such that* $\forall(\rho',\mathbf{J}')\in\mathcal{H}^{\frac{1}{2},-\frac{1}{2}}\times\mathscr{H}_{\mathrm{div}}^{\frac{1}{2},-\frac{1}{2}}$:

$$\langle\ddot{\mathbf{J}}',\mathcal{L}_{\partial_t\mathrm{V}}\{\mathbf{J},\Pi\}\rangle_\sigma=-\left\langle\ddot{\mathbf{J}}',\hat{n}\times(\dot{\mathbf{A}}^{\mathrm{inc}}\times\hat{n})\right\rangle_\sigma \tag{59}$$

and

$$\langle\dddot{\rho}',\mathcal{L}_{\mathrm{S}}\{\mathbf{J},\Pi\}\rangle_\sigma=\left\langle\dddot{\rho}',\Phi^{\mathrm{inc}}\right\rangle_\sigma. \tag{60}$$

Many of the Sobolev spaces in this variational problem follow directly from the discussions in this section. However, the steps to justify the Sobolev space used for Φ^{inc} is more complicated, and warrants further discussion.

The spatial Sobolev space follows by noting that Φ^{inc} should be a solution to the scalar Helmholtz equation, and so it must at least be in $H^1(\omega,\Omega)$, where Ω is some bounded domain external to S [19]. For the purposes of the integral equation, we need to take the trace of Φ^{inc} to determine its value on S. This trace is in the space $H^{\frac{1}{2}}(\omega,S)$ by definition, which establishes the appropriate spatial Sobolev space for Φ^{inc} [19, 35]. This can also be seen alternatively by considering the structure of the pairing, which requires Φ^{inc} to be in the dual space to $\dddot{\rho}'$. Since ρ' acts like a charge density, its spatial Sobolev space is $H^{-\frac{1}{2}}(\omega,S)$, which is dual to $H^{\frac{1}{2}}(\omega,S)$.

In addition to the spatial Sobolev space, the correct temporal order of the Sobolev space also must be determined when transitioning from $\nabla\Phi^{\mathrm{inc}}$ to Φ^{inc}. The reason for this is that the temporal order of functions in electromagnetics is affected by spatial derivatives, in addition to temporal derivatives. Simple motivating examples of this are seen in Maxwell's curl equations and the current continuity equation; however, the concept also applies to the gradient, as seen in [29]. Due to this, it is necessary for Φ^{inc} to be a member of a temporal Sobolev space of one order higher than $\nabla\Phi^{\mathrm{inc}}$. This is further reinforced by the structure of the space-time pairing used for discretizing the integral equation. Transferring the gradient to the testing function resulted in lowering its temporal Sobolev space order to $-5/2$, which is then balanced by an increase in the temporal order of the other function. It is retaining the correct temporal balance between equations and functions in the discretization process that is critical to stability of the method, as will be seen in the coming sections.

3.3. Final Variational Problems

Although Variational Problem 3 constitutes a solvable system in theory, the MOT discretization of it is still problematic. This is because the temporal test space for (59) is $H_{\sigma}^{-\frac{3}{2}}$ and the temporal test space for (60) is $H_{\sigma}^{-\frac{5}{2}}$, i.e., different temporal testing functions should be used for the two equations. As a result, the same discretization approach will not work for the two equations, so they cannot be discretized consistently. To be discretized consistently will require that the two equations have the same temporal testing space. Further, the temporal Sobolev space that an unknown should be a member of should be the same in each equation. If this is not the case, the numerical implementation using traditional discretization approaches (e.g. MOT) may not always be able to produce a robustly stable system. This point will be discussed further in Section 4 when details on discretizing these variational problems are considered.

To correct for the inconsistency in temporal Sobolev spaces between (59) and (60), either equation can be integrated by parts temporally. Due to the presence of the temporal weighting function in the space-time pairings, it will be necessary to consider the effect caused by the additional term produced by differentiating the weighting function. However, as is shown in [27], this additional term can be absorbed into the definition of either the basis or testing function (depending on which is integrated by parts) by adjusting the temporal Sobolev space that the function should be selected from. The overall effect is that a function which has a time derivative transferred off of it will be a member of a temporal Sobolev space of one order higher, while the function that had the time derivative transferred onto it will have the order of its temporal Sobolev space lowered by one.

With this understood, the first variational problem for this section can be derived by integrating by parts to transfer one of the temporal derivatives on the testing function in (60) to the other term in the pairing. This gives the following variational problem, termed the differentiated A-Φ integral equation (D-APIE).

Variational Problem 4. *(Differentiated A-Φ Integral Equation)*
$\forall(\dot{\mathbf{A}}^{\text{inc}}\times\hat{n}) \in \mathscr{H}_{\text{div}}^{\frac{3}{2},-\frac{1}{2}}$ *and* $\forall\dot{\Phi}^{\text{inc}} \in \mathcal{H}^{\frac{3}{2},\frac{1}{2}}$ *search for* $(\Pi, \mathbf{J}) \in \mathcal{H}^{\frac{1}{2},-\frac{1}{2}} \times \mathscr{H}_{\text{div}}^{\frac{1}{2},-\frac{1}{2}}$ *such that* $\forall(\rho', \mathbf{J}') \in \mathcal{H}^{\frac{1}{2},-\frac{1}{2}} \times \mathscr{H}_{\text{div}}^{\frac{1}{2},-\frac{1}{2}}$:

$$\langle\ddot{\mathbf{J}}', \mathcal{L}_{\partial_t \text{V}}\{\mathbf{J}, \Pi\}\rangle_{\sigma} = -\left\langle\ddot{\mathbf{J}}', \hat{n}\times(\dot{\mathbf{A}}^{\text{inc}}\times\hat{n})\right\rangle_{\sigma} \tag{61}$$

and

$$\langle\ddot{\rho}', \mathcal{L}_{\partial_t \text{S}}\{\mathbf{J}, \Pi\}\rangle_{\sigma} = \left\langle\ddot{\rho}', \dot{\Phi}^{\text{inc}}\right\rangle_{\sigma}, \tag{62}$$

where

$$\mathcal{L}_{\partial_t \text{S}}\{\mathbf{J}, \Pi\}(\mathbf{r}, t) = \int_S \left[\frac{\nabla' \cdot \mathbf{J}(\mathbf{r}', \tau)}{4\pi R\epsilon} - \frac{\dot{\Pi}(\mathbf{r}', \tau)}{4\pi R}\right] dS'. \tag{63}$$

As mentioned previously, the importance of this variational problem is that the temporal test spaces are now the same for the two equations, i.e., the physically needed temporal balance between the equations is achieved. This is seen by noting that the temporal test space for (61) is still $H_{\sigma}^{-\frac{3}{2}}$, while the integration by parts has adjusted the temporal test space for (62) to also be $H_{\sigma}^{-\frac{3}{2}}$. Since the temporal basis spaces are also the same for the two unknowns, this variational problem may be discretized consistently. This discretization will be considered in more detail in Section 4, where it will also be seen that the resulting matrix system from the discretization will be symmetric. This is a useful numerical property that can allow for more efficient computation and solution of the matrix system.

Although the D-APIE can be discretized consistently, it may be more desirable to use as excitation the incident potentials directly, as opposed to the time derivatives of them. Additionally, since these are equivalence principle type integral equations, the integral operators on the LHS of the equations calculate the scattered potential that when added to the incident potentials yields the total potential. As a result, it can be seen that the integral operators of the D-APIE will calculate the time derivative of the scattered potentials, which are not quantities that are as physically relevant as the undifferentiated potentials.

A variational problem that is in terms of the incident potentials (as opposed to differentiated ones) can be derived by integrating by parts in (59) to transfer a time derivative from the integral operator and incident potential onto the testing function. This gives the following variational problem, termed the APIE.

Variational Problem 5. *(A-Φ Integral Equation)*
$\forall(\mathbf{A}^{\text{inc}}\times\hat{n}) \in \mathscr{H}_{\text{div}}^{\frac{5}{2},-\frac{1}{2}}$ *and* $\forall\Phi^{\text{inc}} \in \mathcal{H}^{\frac{5}{2},\frac{1}{2}}$ *search for* $(\Pi,\mathbf{J}) \in \mathcal{H}^{\frac{1}{2},-\frac{1}{2}} \times \mathscr{H}_{\text{div}}^{\frac{1}{2},-\frac{1}{2}}$ *such that* $\forall(\rho',\mathbf{J}') \in \mathcal{H}^{\frac{1}{2},-\frac{1}{2}} \times \mathscr{H}_{\text{div}}^{\frac{1}{2},-\frac{1}{2}}$:

$$\langle \ddot{\mathbf{J}}', \mathcal{L}_{\text{V}}\{\mathbf{J},\Pi\}\rangle_\sigma = -\left\langle \ddot{\mathbf{J}}', \hat{n}\times(\mathbf{A}^{\text{inc}}\times\hat{n})\right\rangle_\sigma \tag{64}$$

and

$$\langle \ddot{\rho}', \mathcal{L}_{\text{S}}\{\mathbf{J},\Pi\}\rangle_\sigma = \left\langle \ddot{\rho}', \Phi^{\text{inc}}\right\rangle_\sigma, \tag{65}$$

where

$$\mathcal{L}_{\text{V}}\{\mathbf{J},\Pi\}(\mathbf{r},t) = \int_S \left[\mu\frac{\mathbf{J}(\mathbf{r}',\tau)}{4\pi R} - \nabla\int_{-\infty}^{\tau}\frac{\Pi(\mathbf{r}',t')}{4\pi R}dt'\right]dS'. \tag{66}$$

Following the same discussion as for the D-APIE, it is quickly seen that the temporal test spaces for (64) and (65) are both $H_\sigma^{-\frac{5}{2}}$. As a result, this variational problem can also be discretized consistently, as will be discussed in detail in Section 4.

3.4. Stability

The calculus based approach of the previous sections provided a means of determining the appropriate equations, unknowns, and corresponding Sobolev spaces for the **A**-Φ TDIEs. However, this calculus based approach does not directly provide the desired bounds on the solutions to these problems to demonstrate the stability of the formulation rigorously. This leaves the results of Section 3.3 somewhat incomplete from a mathematical perspective. The focus of this section is to perform the necessary analysis to demonstrate that the two **A**-Φ TDIEs derived in the previous section do still produce a finite amount of electromagnetic energy that is bounded by the incident energy.

To begin, we again consider the scattered electromagnetic energy for the EFIE, which through Parseval's theorem is given as

$$\int_{-\infty}^{\infty} e^{-2\sigma t}\|\mathcal{L}\{\mathbf{J}\}(\cdot,t)\|^2_{H(\text{curl},t,\Omega)}\,dt = \frac{1}{2\pi}\int_{-\infty+i\sigma}^{\infty+i\sigma}\|\mathcal{L}\{\tilde{\mathbf{J}}\}(\cdot,\omega)\|^2_{H(\text{curl},\omega,\Omega)}\,d\omega. \tag{67}$$

Following the derivation of the previous section, it is clear that we can expand the EFIE operator on the RHS as

$$\mathcal{L}\{\tilde{\mathbf{J}}\}(\mathbf{r},\omega) = \mathcal{L}_{\partial_t\text{V}}\{\tilde{\mathbf{J}},\tilde{\Pi}\}(\mathbf{r},\omega) - \nabla\mathcal{L}_{\text{H}}\{\hat{n}'\cdot\nabla'\tilde{\Phi}\}(\mathbf{r},\omega), \tag{68}$$

where

$$\mathcal{L}_{\partial_t\text{V}}\{\tilde{\mathbf{J}},\tilde{\Pi}\}(\mathbf{r},\omega) = -\int_S\left[i\omega\mu\tilde{g}(\mathbf{r},\mathbf{r}')\tilde{\mathbf{J}}(\mathbf{r}') + \nabla\tilde{g}(\mathbf{r},\mathbf{r}')\tilde{\Pi}(\mathbf{r}')\right]dS' \tag{69}$$

and

$$\mathcal{L}_{\text{H}}\{\hat{n}'\cdot\nabla'\tilde{\Phi}\}(\mathbf{r},\omega) = \int_S \tilde{g}(\mathbf{r},\mathbf{r}')\hat{n}'\cdot\nabla'\tilde{\Phi}(\mathbf{r}')\,dS'. \tag{70}$$

Using the triangle inequality we can see that we will need to find bounds for the following two norms,

$$\|\mathcal{L}_{\partial_t\text{V}}\{\tilde{\mathbf{J}},\tilde{\Pi}\}(\cdot,\omega)\|^2_{H(\text{curl},\omega,\Omega)} \tag{71}$$

and

$$\|\nabla\mathcal{L}_{\text{H}}\{\hat{n}'\cdot\nabla'\tilde{\Phi}\}(\cdot,\omega)\|^2_{H(\text{curl},\omega,\Omega)}. \tag{72}$$

To simplify the notation in this section, we will denote $\mathcal{L}_{\text{H}}\{\hat{n}'\cdot\nabla'\tilde{\Phi}\}(\mathbf{r},\omega)$ as $\tilde{\Phi}^{\text{sc}}(\mathbf{r},\omega)$ for the remainder of this discussion. It should also be noted that the integral of the cross terms formed between the above two norms by applying the triangle inequality will also be bounded if we can find bounds for the above norms.

Initially, we will focus on the norm in (72) and apply the process detailed in Section 2.3 to demonstrate that the scattered energy is bounded by the incident energy. The first step of relating the time domain energy to the frequency domain energy has already been completed through the application of Parseval's theorem. The next step is to use properties of the integral operator to bound the scattered energy by the norm of the source function that produced the scattered field.

Considering that the integral operator in (72) is a scalar integral, it will be useful to first find a way to bound (72) by the scalar energy norm. This can be done by first noting that $\nabla\tilde{\Phi}^{\text{sc}}$ is a component of the electric field, and so is a member of $H(\text{curl}, \omega, \Omega) \cap H(\text{div}, \omega, \Omega)$. It is then possible to use one of the results for trace operators of electromagnetic functions given in [29] to conclude that

$$\|\nabla\tilde{\Phi}^{\text{sc}}(\cdot,\omega)\|_{H(\text{curl},\omega,\Omega)} \leq \|\nabla\tilde{\Phi}^{\text{sc}}(\cdot,\omega)\|_{H(\text{div},\omega,\Omega)} \leq C(S)|\omega|^{-\frac{1}{2}}\|\hat{n}\cdot\nabla\tilde{\Phi}^{\text{sc}}(\cdot,\omega)\|_{H^{-\frac{1}{2}}(\omega,S)}. \tag{73}$$

A standard property for the normal derivative trace operator (i.e., $\hat{n}\cdot\nabla$), as give in [19], is that

$$\|\hat{n}\cdot\nabla\tilde{\Phi}^{\text{sc}}(\cdot,\omega)\|_{H^{-\frac{1}{2}}(\omega,S)} \leq C(S,\sigma)\|\tilde{\Phi}^{\text{sc}}(\cdot,\omega)\|_{H^{1}(\omega,\Omega)}. \tag{74}$$

This shows in this context that the trace of a function is bounded by the energy of that function. Further, this process has provided the desired bound on the vector energy norm by the scalar energy norm.

At this point, the properties of the $\mathcal{L}_{\text{H}}$ integral operator can now be used to bound the scalar energy norm of $\tilde{\Phi}^{\text{sc}}$ by the norm of the source function that produced it. As shown in [19], this bound is

$$\|\tilde{\Phi}^{\text{sc}}(\cdot,\omega)\|_{H^{1}(\omega,\Omega)} \leq C(S,\sigma)|\omega|\|\hat{n}'\cdot\nabla'\tilde{\Phi}(\cdot,\omega)\|_{H^{-\frac{1}{2}}(\omega,S)}, \tag{75}$$

which gives overall that

$$\|\nabla\tilde{\Phi}^{\text{sc}}(\cdot,\omega)\|_{H(\text{curl},\omega,\Omega)} \leq C(S,\sigma)|\omega|^{\frac{1}{2}}\|\hat{n}'\cdot\nabla'\tilde{\Phi}(\cdot,\omega)\|_{H^{-\frac{1}{2}}(\omega,S)}. \tag{76}$$

This demonstrates rigorously that $\hat{n}'\cdot\nabla'\Phi \in \mathcal{H}^{\frac{1}{2},-\frac{1}{2}}$, which was previously stated in Section 3.2 with a simplified justification.

The next step to illustrate the stability of the TDIE is to bound (76) by the incident energy. This uses properties of the partial differential equation that the integral equation is related to. For the current problem, the integral equation is

$$\int_S \tilde{g}(\mathbf{r},\mathbf{r}')\hat{n}'\cdot\nabla'\tilde{\Phi}(\mathbf{r}')\,dS' = \tilde{\Phi}^{\text{inc}}(\mathbf{r}), \tag{77}$$

which can be derived through Huygens' principle for a PEC object [37]. This is naturally related to the scalar wave equation, which allows the following bound to be established [19]

$$\|\hat{n}'\cdot\nabla'\tilde{\Phi}(\cdot,\omega)\|_{H^{-\frac{1}{2}}(\omega,S)} \leq C(S,\sigma)|\omega|\|\tilde{\Phi}^{\text{inc}}(\cdot,\omega)\|_{H^{\frac{1}{2}}(\omega,S)}. \tag{78}$$

Although (78) provides the needed bound, it does not account for all of the properties of the problem started with. In particular, the original system being considered had a gradient applied to $\tilde{\Phi}^{\text{inc}}$ which has not been accounted for yet. It was previously mentioned informally that spatial derivatives affect the temporal regularity of electromagnetic functions in the time domain. The explicit property given in [29] with respect to the gradient is that if $f \in H^{s}_{\sigma}(\mathbb{R}_+, H^{m}(\omega,\Omega))$ then $\nabla f \in H^{s-1}_{\sigma}(\mathbb{R}_+, H^{m}(\omega,\Omega)^3)$. As a result, to compensate for "removing" the gradient of $\tilde{\Phi}^{\text{inc}}$ in the above analysis, it will be necessary to require that Φ^{inc} can have an additional temporal derivative applied to it. This can be incorporated into the above bounds by multiplying by an additional factor of $|\omega|$, resulting in the final desired bound of

$$\|\nabla\tilde{\Phi}^{\text{sc}}(\cdot,\omega)\|_{H(\text{curl},\omega,\Omega)} \leq C(S,\sigma)|\omega|^{\frac{5}{2}}\|\tilde{\Phi}^{\text{inc}}(\cdot,\omega)\|_{H^{\frac{1}{2}}(\omega,S)}. \tag{79}$$

This also serves the purpose of demonstrating that Φ^{inc} should be in $\mathcal{H}^{\frac{5}{2},\frac{1}{2}}$, as was previously asserted in Section 3.2.

Our task is now to extend this result to cover the equations actually used, i.e., for

$$\|\mathcal{L}_{\mathrm{H}}\left\{\frac{\nabla' \cdot \tilde{\mathbf{J}}}{i\omega}\right\}(\cdot,\omega)\|_{H^1(\omega,\Omega)} \tag{80}$$

and

$$\|\mathcal{L}_{\mathrm{H}}\{\tilde{\Pi}\}(\cdot,\omega)\|_{H^1(\omega,\Omega)}. \tag{81}$$

However, bounds on both of these norms come immediately from the above discussion by recalling that this norm is directly related to the energy in the region Ω. So, for physical reasons we know that the upper bound in (75) will also upper bound (80) and (81).

In addition to the overall bounds above, it is useful to write the bounds on the source functions themselves like was done for the EFIE. For instance,

$$\|\tilde{\Pi}(\cdot,\omega)\|_{H^{-\frac{1}{2}}(\omega,S)} \leq C(S,\sigma)|\omega|^2\|\tilde{\Phi}^{\mathrm{inc}}(\cdot,\omega)\|_{H^{\frac{1}{2}}(\omega,S)}, \tag{82}$$

which in the time domain becomes

$$\|\Pi\|_{\mathcal{H}^{\frac{1}{2},-\frac{1}{2}}} \leq C(S,\sigma)\|\dot{\Phi}^{\mathrm{inc}}\|_{\mathcal{H}^{\frac{3}{2},\frac{1}{2}}} = C(S,\sigma)\|\Phi^{\mathrm{inc}}\|_{\mathcal{H}^{\frac{5}{2},\frac{1}{2}}}. \tag{83}$$

These bounds can then be used to compactly demonstrate the stability of the overall system, as will be seen shortly.

A similar process to what was outlined above for bounding (72) could also be conducted for establishing bounds on (71). However, it is simpler to note that the operator is the same as the EFIE operator in (37), so the same bounds will hold (although, the physical interpretation does change). This gives the following additional bounds:

$$\|\mathbf{J}\|_{\mathscr{H}_{\mathrm{div}}^{\frac{1}{2},-\frac{1}{2}}} \leq C(S,\sigma)\|\dot{\mathbf{A}}^{\mathrm{inc}}\times\hat{n}\|_{\mathscr{H}_{\mathrm{div}}^{\frac{3}{2},-\frac{1}{2}}} = C(S,\sigma)\|\mathbf{A}^{\mathrm{inc}}\times\hat{n}\|_{\mathscr{H}_{\mathrm{div}}^{\frac{5}{2},-\frac{1}{2}}} \tag{84}$$

and

$$\|\Pi\|_{\mathcal{H}^{\frac{1}{2},-\frac{1}{2}}} \leq C(S,\sigma)\|\dot{\mathbf{A}}^{\mathrm{inc}}\times\hat{n}\|_{\mathscr{H}_{\mathrm{div}}^{\frac{3}{2},-\frac{1}{2}}} = C(S,\sigma)\|\mathbf{A}^{\mathrm{inc}}\times\hat{n}\|_{\mathscr{H}_{\mathrm{div}}^{\frac{5}{2},-\frac{1}{2}}}. \tag{85}$$

Combining all of these results, we can now give the final bounds which demonstrate the stability of the variational problems for the APIE and the D-APIE. For the APIE, we have

$$\|\mathbf{J}\|_{\mathscr{H}_{\mathrm{div}}^{\frac{1}{2},-\frac{1}{2}}} \leq C(S,\sigma)\left(\|\mathbf{A}^{\mathrm{inc}}\times\hat{n}\|_{\mathscr{H}_{\mathrm{div}}^{\frac{5}{2},-\frac{1}{2}}} + \|\Phi^{\mathrm{inc}}\|_{\mathcal{H}^{\frac{5}{2},-\frac{1}{2}}}\right) \tag{86}$$

$$\|\Pi\|_{\mathcal{H}^{\frac{1}{2},-\frac{1}{2}}} \leq C(S,\sigma)\left(\|\mathbf{A}^{\mathrm{inc}}\times\hat{n}\|_{\mathscr{H}_{\mathrm{div}}^{\frac{5}{2},-\frac{1}{2}}} + \|\Phi^{\mathrm{inc}}\|_{\mathcal{H}^{\frac{5}{2},-\frac{1}{2}}}\right). \tag{87}$$

Finally, for the D-APIE we have

$$\|\mathbf{J}\|_{\mathscr{H}_{\mathrm{div}}^{\frac{1}{2},-\frac{1}{2}}} \leq C(S,\sigma)\left(\|\dot{\mathbf{A}}^{\mathrm{inc}}\times\hat{n}\|_{\mathscr{H}_{\mathrm{div}}^{\frac{3}{2},-\frac{1}{2}}} + \|\dot{\Phi}^{\mathrm{inc}}\|_{\mathcal{H}^{\frac{3}{2},-\frac{1}{2}}}\right) \tag{88}$$

$$\|\Pi\|_{\mathcal{H}^{\frac{1}{2},-\frac{1}{2}}} \leq C(S,\sigma)\left(\|\dot{\mathbf{A}}^{\mathrm{inc}}\times\hat{n}\|_{\mathscr{H}_{\mathrm{div}}^{\frac{3}{2},-\frac{1}{2}}} + \|\dot{\Phi}^{\mathrm{inc}}\|_{\mathcal{H}^{\frac{3}{2},-\frac{1}{2}}}\right). \tag{89}$$

Although these may not be the *minimal* bounds for $\mathbf{J}$ and Π, they have been written in a symmetric form which emphasizes that they are both bounded by the incident potentials, as desired.

3.5. Original A-Φ Formulation Variational Problem

Before discussing the full details of discretizing these variational problems, it is useful to revisit the original **A**-Φ formulation integral equations discussed in Section 3.1 within the functional framework utilized throughout this work. This is useful to begin demonstrating how no suitable MOT discretization scheme can be derived for this formulation in the time domain to yield stable results. Further, studying the variational problem for this formulation also helps highlight the utility of this functional framework in selecting correct basis and testing functions, equations, and unknowns when the choice is not directly obvious.

Before presenting the variational problem, it is necessary to convert (43) and (45) to the time domain. This can be done easily, and gives

$$\int_S \left[\mu \frac{\mathbf{J}(\mathbf{r}',\tau)}{4\pi R} - \nabla \frac{\Sigma(\mathbf{r}',\tau)}{4\pi R}\right] dS' = -\mathbf{A}^{\text{inc}}(\mathbf{r},t) \tag{90}$$

$$\int_S \left[\frac{\nabla' \cdot \mathbf{J}(\mathbf{r}',\tau)}{4\pi R\epsilon} - \frac{\ddot{\Sigma}(\mathbf{r}',\tau)}{4\pi R}\right] dS' = \dot{\Phi}^{\text{inc}}(\mathbf{r},t). \tag{91}$$

The corresponding variational problem can be derived in a similar manner to the others presented in this work. Performing this gives the following variational problem.

Variational Problem 6. *(Original Formulation)*
$\forall(\mathbf{A}^{\text{inc}}\times\hat{n}) \in \mathscr{H}_{\text{div}}^{\frac{5}{2},-\frac{1}{2}}$ *and* $\forall\dot{\Phi}^{\text{inc}} \in \mathcal{H}^{\frac{3}{2},\frac{1}{2}}$ *search for* $(\Sigma,\mathbf{J}) \in \mathcal{H}^{\frac{3}{2},-\frac{1}{2}} \times \mathscr{H}_{\text{div}}^{\frac{1}{2},-\frac{1}{2}}$ *such that* $\forall(\rho',\mathbf{J}') \in \mathcal{H}^{\frac{1}{2},-\frac{1}{2}} \times \mathscr{H}_{\text{div}}^{\frac{1}{2},-\frac{1}{2}}$:

$$\left\langle \dddot{\mathbf{J}}', \int_S \left[\mu \frac{\mathbf{J}(\mathbf{r}',\tau)}{4\pi R} - \nabla \frac{\Sigma(\mathbf{r}',\tau)}{4\pi R}\right] dS' \right\rangle_\sigma = -\left\langle \dddot{\mathbf{J}}', \hat{n}\times(\mathbf{A}^{\text{inc}}\times\hat{n}) \right\rangle_\sigma \tag{92}$$

and

$$\left\langle \ddot{\rho}', \int_S \left[\frac{\nabla' \cdot \mathbf{J}(\mathbf{r}',\tau)}{4\pi R\epsilon} - \frac{\ddot{\Sigma}(\mathbf{r}',\tau)}{4\pi R}\right] dS' \right\rangle_\sigma = \left\langle \ddot{\rho}', \dot{\Phi}^{\text{inc}} \right\rangle_\sigma . \tag{93}$$

From past discussions, it is clear that the temporal test space for (92) is $H_\sigma^{-\frac{5}{2}}$ and the temporal test space for (93) is $H_\sigma^{-\frac{3}{2}}$. As a result, these two equations cannot be discretized consistently within a MOT framework, as will be shown in Section 4. This is critical, since the MOT framework is what is traditionally utilized and is the method that has had suitable fast algorithms developed for it. Further, from the variational formulation it is also seen that the temporal basis functions for the two unknowns should be different. Although not impossible to implement, it would complicate the numerical implementation. More importantly, however, is that without the use of the functional framework it would not be immediately obvious that different temporal basis functions for the two unknowns or different equations should have been used at all.

4. MOT Discretization of Variational Problems

The focus of this section is making explicit the steps needed to discretize the variational problems discussed throughout this work. In particular, a number of general concepts are discussed that clarify how basis and testing functions should be selected to achieve a stable MOT discretization. Following this, the discretized equations for the APIE and the D-APIE are presented.

4.1. MOT Procedure

Before discussing how information from the variational problems derived in this work can be used to produce a stable discretized system, we briefly review the MOT discretization procedure. This is the method commonly used to solve TDIEs in the literature due to the existence of fast algorithms that can be merged with this approach to greatly improve the computational complexity [17]. As a result, it is highly desirable to find a way to use the information from variational problems to achieve a MOT system that will be stable in practice.

The first step of a MOT discretization is to expand the unknown functions in terms of known basis functions. For the different APIEs this can be written as

$$\mathbf{J}(\mathbf{r}',t) \approx \sum_{n=1}^{N_s}\sum_{j=1}^{N_t} J_n^{(j)} T^{(j)}(t)\mathbf{f}_n(\mathbf{r}') \tag{94}$$

$$\Pi(\mathbf{r}',t) \approx \sum_{n=1}^{N_p}\sum_{j=1}^{N_t} \psi_n^{(j)} T^{(j)}(t) h_n(\mathbf{r}'). \tag{95}$$

In (94), $\mathbf{f}_n$ is a vector spatial function associated with the nth mesh element (e.g., interior edges) that the selected function is defined with respect to. Similarly, h_n is scalar spatial function which may be defined over a different type of mesh element than $\mathbf{f}_n$ (e.g., h_n could be defined over a triangle). The total number of mesh elements that $\mathbf{f}_n$ is defined for is N_s, while N_p is similar but defined for h_n. This leads to a total number of spatial unknowns to be $N_s + N_p$, i.e., the different matrices of the MOT system will be $(N_s + N_p) \times (N_s + N_p)$. The temporal basis function is $T^{(j)}(t) = T(t - j\Delta t)$, where Δt is the width of each time step of the simulation, and N_t is the total number of time steps. Finally, $J_n^{(j)}$ and $\psi_n^{(j)}$ are the coefficients of the basis expansion to be solved for at each time step.

After substituting the basis expansions of (94) and (95) into the different equations, the next step of the MOT discretization is to test the equations. The spatial testing is performed in a manner similar to frequency domain methods, e.g. multiplying by another spatial function and integrating over the surface with respect to $\mathbf{r}$. The time domain testing is done by point matching, i.e., multiplying by $\delta(t - i\Delta t)$ and integrating over t (which enforces the equations at an instant in time).

The result of this is a system of equations that can be used to solve for the unknown coefficients at the current time step in terms of the current excitation (incident potentials for the APIEs) and the radiated potentials from earlier time steps. This is the time marching process to compute the unknowns throughout the entire run time of the simulation.

4.2. General Concepts

With the basic MOT procedure now understood, the focus of this section is on showing how information from the variational problems can be used to determine correct basis and testing functions that will lead to MOT systems that will be stable in practice.

To begin, the selection of appropriate spatial basis and testing functions is considered. Inspection of the variational problems for the APIE and the D-APIE show that the appropriate spatial Sobolev space for $\mathbf{J}$ is $H^{-\frac{1}{2}}(\mathrm{div}, S)$ and the correct space for Π is $H^{-\frac{1}{2}}(S)$. From Table 1, it is seen that suitable basis functions are then RWG and pulse functions, respectively. Similarly, it is seen that the appropriate testing functions for (61) and (64) are RWG functions, and that pulse functions should be used to test (62) and (65). Other options do exist for the spatial discretization [27]; however, these are the only functions that will be used in this work.

Although the spatial discretization is quite simple, the temporal discretization is more nuanced. To begin, we consider the D-APIE, as this variational problem is simpler to discretize. The first step is again to determine the relevant temporal Sobolev spaces for each equation. For the D-APIE, it is seen that the correct temporal basis space is $H_\sigma^{\frac{1}{2}}$ for both $\mathbf{J}$ and Π. From Table 2, it is determined that the simplest temporal basis function that is a member of this space is a triangular function. Recalling the discussion after Variational Problem 4, it is identified that the temporal testing space for the D-APIE is $H_\sigma^{-\frac{3}{2}}$. The simplest function in this space is the Dirac delta function, which directly leads to the MOT procedure.

At this point, it is important to note a detail related to the nesting properties of the Sobolev spaces. In particular, it is easy to see that $H_\sigma^{s+1} \subset H_\sigma^s$. In the context of the D-APIE, this would mean that any function in $H_\sigma^{\frac{3}{2}}$ is also in $H_\sigma^{\frac{1}{2}}$, and could then conceivably be used as a basis function. However, numerical results have suggested that this should not be done as it can lead to instability in the system. The exact reason for this is currently unknown, however, one possible reason is that $H_\sigma^{\frac{3}{2}}$ is a subspace of $H_\sigma^{\frac{1}{2}}$. As a result, in the process of the numerical method, the solution is being projected onto a smaller space than where the solution should be sought in. The resulting error incurred is then fed back into the system through the MOT procedure, which could lead to unstable results. The instability due to using basis functions from a subspace will be demonstrated in Section 5. Before continuing, we emphasize that

these comments are based on observations of non-exhaustive numerical results. For example, we have not explored utilizing other numerical integration techniques beyond those detailed in Section 4.3.

With this in mind, we can now begin to consider the discretization of the APIE. The Sobolev spaces for $\mathbf{J}$ and Π are the same as in the D-APIE; so it is originally expected that using a triangular basis function would be appropriate. However, the temporal testing spaces are different from the D-APIE and are seen to be $H_\sigma^{-\frac{5}{2}}$. Inspecting Table 2 shows that a function in $H_\sigma^{-\frac{5}{2}}$ would look like the derivative of a Dirac delta function. Attempting to use a function like this directly would not lead to a MOT discretization; so it is not desired to conduct the discretization in this way.

Instead, it is noted that an equivalent MOT discretization can be found by using a basis function that comes from convolving functions from the basis and testing temporal Sobolev spaces for the original problem [45, 46]. If we were to use the simplest functions in these spaces in this way (a derivative of a Dirac delta and a triangular function), the resulting system would be identical to the D-APIE. To avoid this, we instead choose to enforce this relationship at a higher functional level. In particular, it is anticipated that convolving a general element of $H_\sigma^{-\frac{5}{2}}$ with one in $H_\sigma^{\frac{1}{2}}$ would lead to a function in $H_\sigma^{-\frac{1}{2}}$. From this, we choose to discretize the APIE with a rectangular function as the temporal basis function. As will be shown in Section 5, this does lead to a stable system.

It is also important to note that similar to the Sobolev space nesting properties discussed in conjunction with the discretization of the D-APIE, a similar concept also applies to the APIE. In particular, it is noted that $H_\sigma^{-\frac{3}{2}} \subset H_\sigma^{-\frac{5}{2}}$. This means that a Dirac delta could be used as the testing function directly to discretize the APIE using a MOT procedure with a triangular temporal basis function. However, as with the D-APIE, numerical results suggest that the largest appropriate Sobolev space should be used, not a smaller subspace. As will be shown in Section 5, attempting to do this direct MOT discretization leads to unstable results for the APIE. As a result, the more detailed procedure outlined in the previous paragraphs should be considered instead. This also illustrates why equations that require different temporal testing spaces are not able to be discretized together consistently in a MOT framework. From this discussion, it is seen that different temporal basis functions would be required for each equation, which would result in more unknowns than can be solved for.

A final remark for discretizing the variational formulations is required for the choice of σ. For computational efficiency reasons, this value should be zero. However, the stability results of the functional framework are only technically valid for $\sigma > 0$ [19, 27]. As a result, the stability proofs do not extend directly to the desired numerical implementation. In practice, however, it has been found that as long as the basis and testing functions have been selected from the relevant Sobolev spaces and accurate integration techniques are used to compute the MOT matrix elements, the methods are stable enough to be widely used [19, 27, 47].

4.3. Accurate Evaluation of the Matrix Elements

A necessary but not sufficient condition for the stability of a MOT-discretized TDIE is that the matrix elements be accurately evaluated [27]. Various methods have been developed to do this, with the most popular being those of [23, 24, 25]. All of these methods have produced accurate results, and due to the similarity in integral operators between the **A**-Φ and **E**-**H** TDIEs, are directly applicable to the TDIEs derived throughout this work. However, the method presented in [25] was selected for use because of its ease of implementation for arbitrary basis functions. This is a result of the method being purely numerical (i.e., no analytical integrations need be derived as in [23, 24]) which allows it to be applied to a wide range of basis functions. In contrast, the methods of [23, 24] are designed specifically for RWG functions and would be very challenging to extend to other basis functions if needed.

Due to its impact on the final discretized equations presented in Sections 4.4 and 4.5, the basics of the method presented in [25] are discussed in this section. This provides both completeness and clarity so that various terms in the discretized equations can be understood.

The approach of [25] is to approximate the time domain Green's function,

$$g(\mathbf{r}, \mathbf{r}', t) = \frac{\delta(t - R/c)}{4\pi R}, \tag{96}$$

using an expansion that is separable in the spatial and temporal domains. This is done by leveraging the completeness

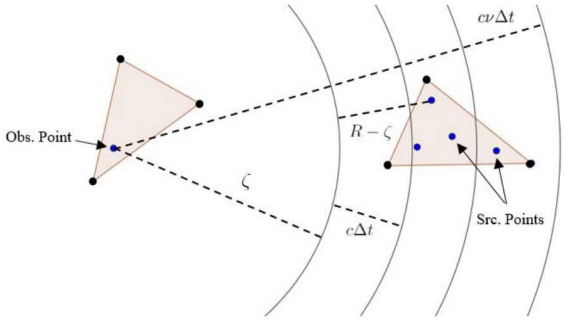

Fig. 1: Geometry defining the various parameters used in the separable expansion of the Green's function.

relation for the Legendre polynomials,

$$\sum_{l=0}^{\infty} \frac{2l+1}{2} P_l(x')P_l(x) = \delta(x-x'), \tag{97}$$

where P_l is the Legendre polynomial of degree l. By using this expansion for the delta function in (96), the numerical integrations needed for evaluating matrix elements can be greatly simplified. This is because the temporal and spatial integrals can be evaluated almost independently of each other.

With the basic approach understood, we now consider the actual factorization of the Green's function. This is performed first by limiting the total temporal support that the separable expansion will cover. This is done by

$$g(\mathbf{r},\mathbf{r}',t) = \frac{1}{4\pi R}\delta(t-\zeta/c) * \delta\Big(t-\frac{R-\zeta}{c}\Big), \tag{98}$$

where the additional convolution with $\delta(t-\zeta/c)$ limits the support of the separable expansion. In particular, ζ is selected to be the largest multiple of $c\Delta t$ between an observation (testing) quadrature point and the source triangle that the expansion is being performed over, as illustrated in Fig. 1. By limiting the separable expansion to be performed over a smaller temporal support, quicker convergence to an acceptable accuracy level in the series expansion is achieved.

The next step is to apply the separable expansion to the second delta function in (98), giving

$$g(\mathbf{r},\mathbf{r}',t) \approx \delta(t-\zeta/c) * \sum_{l=0}^{N_h} a_l P_l(b\,t-1)\frac{P_l(\tilde{R})}{4\pi R}, \tag{99}$$

where $\tilde{R} = b(R-\zeta)/c - 1$, $a_l = b(2l+1)/2$, and the sum has been truncated to N_h terms for numerical implementation. In (99),

$$b = \frac{2}{\nu\Delta t}, \tag{100}$$

which is used to normalize the argument of the Legendre polynomials so that they cover the entire range of -1 to 1 over the integration region. To achieve this, ν is calculated as the smallest integer such that a sphere with radius $c\nu\Delta t$ centered at the observation point will completely enclose the source triangle (see Fig. 1). Numerical experiments suggest that selecting $N_h = 3(\nu - \zeta/(c\Delta t))$ provides acceptable results [25].

The critical result of this expansion is that the temporal and spatial integrals in the TDIEs can now be evaluated almost independently. This allows frequency domain methods to be utilized for the spatial integrals, e.g., [48]. The temporal integrals can also be easily handled with one-dimensional Gaussian quadrature. With this expansion understood, the discretized equations of the two APIEs presented in this work can be discussed.

4.4. Discretized Equations for the D-APIE

For practical purposes, it is useful to perform some rescaling of the different equations in the D-APIE. This results in a symmetric matrix system, as well as gives it a saddle point form similar to the A-EFIE, which can be effectively and efficiently preconditioned for large problems [15, 49]. The matrix system can be compactly written as

$$\begin{bmatrix} \mu_r \Delta t \dot{\mathbf{V}}^{(0)} & \mathbf{D}^{\mathrm{T}}\mathbf{S}^{(0)} \\ \mathbf{S}^{(0)}\mathbf{D} & -\frac{\epsilon_r}{c_0^2 \Delta t}\dot{\mathbf{S}}^{(0)} \end{bmatrix} \begin{Bmatrix} (c_0\Delta t)^{-1}\mathbf{J}^{(i)} \\ \eta_0^{-1}\boldsymbol{\psi}^{(i)} \end{Bmatrix} = \begin{Bmatrix} -\eta_0^{-1}\dot{\boldsymbol{\alpha}}^{(i)} \\ \frac{\epsilon}{c_0\Delta t}\dot{\boldsymbol{\phi}}^{(i)} \end{Bmatrix} - \sum_{j=i-j_{max}}^{i-1} \begin{bmatrix} \mu_r \Delta t \dot{\mathbf{V}}^{(i-j)} & \mathbf{D}^{\mathrm{T}}\mathbf{S}^{(i-j)} \\ \mathbf{S}^{(i-j)}\mathbf{D} & -\frac{\epsilon_r}{c_0^2 \Delta t}\dot{\mathbf{S}}^{(i-j)} \end{bmatrix} \begin{Bmatrix} (c_0\Delta t)^{-1}\mathbf{J}^{(j)} \\ \eta_0^{-1}\boldsymbol{\psi}^{(j)} \end{Bmatrix}, \tag{101}$$

where η_0 is the intrinsic impedance of free space, c_0 is the speed of light in free space, and Δt is the time step used in the discretization. Note that to write the MOT matrix system in this simple form requires the use of causal basis functions, i.e., $T(t) = 0$ for $t \leq -\Delta t$, which will be the case for all temporal basis functions used in this work. Approaches using non-causal basis functions have also been investigated, but will not be considered here [21].

The different elements of (101) will be defined in more detail later in this section, after discussing the basic structure first. The first point to note is that the matrices with a superscript (0) are typically highly sparse (although, not at low frequencies or for very dense meshes), and represent the immediate interaction between basis and testing functions within the first time step that a function is active. On the RHS of the equation, there are essentially two terms. The first is the excitation of the problem due to the incident potentials, while the second term (a summation of matrix-vector products) accounts for the scattered potentials moving through the geometry as time progresses. It is also important to note that the number of terms in this summation is limited by the number of time steps that it takes for information to propagate between the two furthest separated basis and testing functions. Evaluating this summation is often the most time consuming step in solving the system at each time step, and is what fast algorithms have been developed to speed up [17].

With the structure of the MOT system understood, we now give the detailed definitions for the different terms in (101). The matrix elements are defined as:

$$[\dot{\mathbf{V}}^{(i-j)}]_{mn} = \int_{S_m}\int_{S_n} \sum_{l=0}^{N_h} a_l \dot{\xi}_l^{(i-j)} \mathbf{f}_m(\mathbf{r}) \cdot \mathbf{f}_n(\mathbf{r}') \frac{P_l(\tilde{R})}{4\pi R} dS' dS, \tag{102}$$

$$[\mathbf{S}^{(i-j)}]_{mn} = \int_{T_m}\int_{T_n} \sum_{l=0}^{N_h} a_l \xi_l^{(i-j)} h_m(\mathbf{r}) h_n(\mathbf{r}') \frac{P_l(\tilde{R})}{4\pi R} dS' dS, \tag{103}$$

$$[\dot{\mathbf{S}}^{(i-j)}]_{mn} = \int_{T_m}\int_{T_n} \sum_{l=0}^{N_h} a_l \dot{\xi}_l^{(i-j)} h_m(\mathbf{r}) h_n(\mathbf{r}') \frac{P_l(\tilde{R})}{4\pi R} dS' dS, \tag{104}$$

where the temporal convolutions are contained in

$$\xi_l^{(i-j)} = \int_{-\infty}^{\infty} P_l(b\,t' - 1) T(\kappa - t') dt' \tag{105}$$

$$\dot{\xi}_l^{(i-j)} = \int_{-\infty}^{\infty} P_l(b\,t' - 1) \dot{T}(\kappa - t') dt', \tag{106}$$

and $\kappa = (i-j)\Delta t - \zeta/c$. In these equations, S_n is the support covered by the nth RWG function, T_n is the support of the nth triangle, and T is the temporal basis function. As mentioned in Section 4.2, a simple temporal basis function that will lead to a stable system is a triangle function, i.e.,

$$T(t) = \begin{cases} 1 - \dfrac{|t|}{\Delta t}, & \text{for } |t| \leq \Delta t \\ 0, & \text{elsewhere.} \end{cases} \tag{107}$$

The **D** matrix (also called the incidence matrix) is used to account for the bookkeeping related to taking the divergence of the RWG functions. The matrix is simple and is given by

$$[\mathbf{D}]_{mn} = \begin{cases} 1, & \text{patch of } h_m \text{ is the positive triangle of } \mathbf{f}_n \\ -1, & \text{patch of } h_m \text{ is the negative triangle of } \mathbf{f}_n \\ 0, & \text{otherwise.} \end{cases} \tag{108}$$

Finally, the excitations may be calculated as

$$\{\dot{\boldsymbol{\alpha}}^{(i)}\}_m = \int_{S_m} \mathbf{f}_m(\mathbf{r}) \cdot \dot{\mathbf{A}}^{\text{inc}}(\mathbf{r}, i\Delta t) dS \tag{109}$$

$$\{\dot{\boldsymbol{\phi}}^{(i)}\}_m = \int_{T_m} h_m(\mathbf{r}) \dot{\Phi}^{\text{inc}}(\mathbf{r}, i\Delta t) dS. \tag{110}$$

4.5. Discretized Equations for the APIE

The presence of additional temporal integrals in the APIE complicates its discretization. Care must be taken in the discretization of these integrals to not increase the computational complexity of the entire method due to the "infinite" tails of these integrals. Fortunately, integrals of this type are also present in the EFIE. As a result, mature methods to efficiently evaluate these types of integrals through a recursive computation have already been developed. Applying this recursive approach, which is detailed in more depth in [25], yields the following matrix system:

$$\begin{bmatrix} \mu\mathbf{V}^{(0)} & \mathbf{D}^{\mathrm{T}}\hat{\mathbf{S}}^{(0)} \\ \hat{\mathbf{S}}^{(0)}\mathbf{D} & -\epsilon\mathbf{S}^{(0)} \end{bmatrix} \begin{Bmatrix} \mathbf{J}^{(i)} \\ \boldsymbol{\psi}^{(i)} \end{Bmatrix} = \begin{Bmatrix} -\boldsymbol{\alpha}^{(i)} \\ \epsilon\boldsymbol{\phi}^{(i)} \end{Bmatrix} - \sum_{j=i-j_{max}}^{i-1} \begin{bmatrix} \mu\mathbf{V}^{(i-j)} & \mathbf{D}^{\mathrm{T}}\hat{\mathbf{S}}^{(i-j)} \\ \hat{\mathbf{S}}^{(i-j)}\mathbf{D} & -\epsilon\mathbf{S}^{(i-j)} \end{bmatrix} \begin{Bmatrix} \mathbf{J}^{(j)} \\ \boldsymbol{\psi}^{(j)} \end{Bmatrix} - \sum_{j=i-(j_{\max}+1)}^{i-p-1} \begin{bmatrix} \mathbf{0} & \mathbf{D}^{\mathrm{T}}\hat{\mathbf{S}}_T^{(i-j)} \\ \hat{\mathbf{S}}_T^{(i-j)}\mathbf{D} & \mathbf{0} \end{bmatrix} \begin{Bmatrix} \mathbf{C}_{\mathbf{J}}^{(j+1)} \\ \mathbf{C}_{\boldsymbol{\psi}}^{(j+1)} \end{Bmatrix}. \tag{111}$$

This system has a structure similar to that of the D-APIE, however, it is seen that there is an additional term on the RHS of (111). This summation of matrix vector products represents the recursive computation that handles the "infinite" tails of the off-diagonal blocks of the system. Other than this, the physical interpretation of the other components of this matrix system are unchanged from the D-APIE.

The different matrix elements are defined as:

$$[\mathbf{V}^{(i-j)}]_{mn} = \int_{S_m} \int_{S_n} \sum_{l=0}^{N_h} a_l \xi_l^{(i-j)} \mathbf{f}_m(\mathbf{r}) \cdot \mathbf{f}_n(\mathbf{r}') \frac{P_l(\tilde{R})}{4\pi R} dS' dS, \tag{112}$$

$$[\hat{\mathbf{S}}^{(i-j)}]_{mn} = \int_{T_m} \int_{T_n} \sum_{l=0}^{N_h} a_l \tilde{\xi}_l^{(i-j)} h_m(\mathbf{r}) h_n(\mathbf{r}') \frac{P_l(\tilde{R})}{4\pi R} dS' dS, \tag{113}$$

$$[\hat{\mathbf{S}}_T^{(i-j)}]_{mn} = \int_{T_m} \int_{T_n} \sum_{l=0}^{N_h} a_l \tilde{\xi}_l^{(i-j)} h_m(\mathbf{r}) h_n(\mathbf{r}') \frac{P_l(\tilde{R})}{4\pi R} dS' dS, \tag{114}$$

and the definition for [**S**] has already been given in (103). The temporal integrals are given by

$$\tilde{\xi}_l^{(i-j)} = \int_{-\infty}^{\infty} P_l(b\,t' - 1) \int_{-\infty}^{\kappa - t'} T(t'') dt'' dt', \tag{115}$$

for $\kappa/\Delta t - \nu \leq p$, and

$$\bar{\xi}_l^{(i-j)} = \delta_{l0}\nu\Delta t, \text{ for } p \leq \kappa/\Delta t - \nu \leq (p+1), \tag{116}$$

where the support of T is $[-\Delta t, p\Delta t]$. Note that δ_{l0} is a Kronecker delta function. Additionally, the equation for ξ given in (105) remains the same for the APIE. The vector for the recursive computation is calculated as

$$\begin{Bmatrix} \mathbf{C}_{\mathbf{J}}^{(j+1)} \\ \mathbf{C}_{\boldsymbol{\psi}}^{(j+1)} \end{Bmatrix} = \begin{Bmatrix} \mathbf{C}_{\mathbf{J}}^{(j)} \\ \mathbf{C}_{\boldsymbol{\psi}}^{(j)} \end{Bmatrix} + \begin{Bmatrix} \mathbf{J}^{(j)} \\ \boldsymbol{\psi}^{(j)} \end{Bmatrix} \int_{-\infty}^{\infty} T(t'')dt'', \tag{117}$$

which is begun by setting

$$\begin{Bmatrix} \mathbf{C}_{\mathbf{J}}^{(1)} \\ \mathbf{C}_{\boldsymbol{\psi}}^{(1)} \end{Bmatrix} = \begin{Bmatrix} \mathbf{0} \\ \mathbf{0} \end{Bmatrix}. \tag{118}$$

As discussed in Section 4.2, the temporal basis function that will be used for this system is a square pulse, i.e.,

$$T(t) = \begin{cases} 1, & \text{for } |t| \leq \Delta t \\ 0, & \text{elsewhere.} \end{cases} \tag{119}$$

Finally, the excitations may be calculated as

$$\{\boldsymbol{\alpha}^{(i)}\}_m = \int_{S_m} \mathbf{f}_m(\mathbf{r}) \cdot \mathbf{A}^{\text{inc}}(\mathbf{r}, i\Delta t)dS \tag{120}$$

$$\{\boldsymbol{\phi}^{(i)}\}_m = \int_{T_m} h_m(\mathbf{r})\Phi^{\text{inc}}(\mathbf{r}, i\Delta t)dS. \tag{121}$$

5. Numerical Results

In this section, numerical examples are presented to validate the various claims of stability or instability made throughout this work for the different sets of equations or choices of basis and testing functions. A number of these results are also presented in [16]. They are reproduced here and discussed within the greater context of the functional analysis presented in this work, which was absent from [16].

For all simulations considered, the scatterer is a PEC sphere with a radius of 1 meter unless stated otherwise. This is a very simple shape that would be considered to be "easy" to stabilize using traditional stabilization approaches, e.g., by filtering the marching process [50]. Hence, when systems are shown to be unstable for this simple geometry, it implies that the formulation will be unstable for most other problems. As a result, these simulations are very useful in validating claims of instability based on the functional framework. Note that in order to show a larger diversity of simulations, the incident potential is changed when demonstrating the stability/instability of different formulations. However, all formulations have been run for all simulations settings presented with consistent results achieved. That is, if the formulation is stable (unstable) for one case, it was stable (unstable) for all simulations.

All examples presented here will be for plane wave scattering. Since the excitation is assumed to come from the far-field, Φ^{inc} can be set to zero [15]. The incident vector potential is then taken to be a plane wave with temporal shape defined by a modulated Gaussian pulse,

$$\mathbf{F}^{\text{inc}}(\mathbf{r}, t) = \mathbf{F}_0 \exp\Big[-\Big(\frac{t_r - t_p}{\sqrt{2}\sigma_t}\Big)^2 \Big] \cos(2\pi f_0 t_r). \tag{122}$$

In (122), $\mathbf{F}^{\text{inc}}$ should be the appropriate excitation for the TDIE considered, e.g., $\mathbf{A}^{\text{inc}}$ or $\dot{\mathbf{A}}^{\text{inc}}$. The polarization direction and amplitude are set by $\mathbf{F}_0$, and $t_r = t - \mathbf{r} \cdot \hat{\mathbf{k}}/c$, where $\hat{\mathbf{k}}$ sets the propagation direction. The width of the pulse is set by $\sigma_t = 3/(2\pi f_{\text{bw}})$, where f_{bw} defines the bandwidth of the pulse. Finally, $t_p = 8\sigma_t$ and f_0 is the center

frequency of the pulse. For all sphere simulations, the polarization is in the $\hat{\mathbf{x}}$ direction and the propagation direction is in the $\hat{\mathbf{z}}$ direction. The time step for the simulations is selected to be a fixed oversampling of the Nyquist frequency. This is done by setting $\Delta t = 1/(s(f_0 + f_{bw}))$, where s is usually set between 10 to 20.

To rigorously test the stability of the numerical methods, an eigenvalue stability analysis of the marching system is performed for each simulation [51]. To perform this analysis, a single matrix system must be devised that captures the complete time marching process. The structure of this matrix system can be easily derived, and is

$$\begin{Bmatrix} \mathbf{U}^{(i+1)} \\ \mathbf{U}^{(i)} \\ \mathbf{U}^{(i-1)} \\ \vdots \\ \mathbf{U}^{(i-j_{\max}+3)} \\ \mathbf{U}^{(i-j_{\max}+2)} \end{Bmatrix} = \begin{bmatrix} \mathbf{B}^{(1)} & \mathbf{B}^{(2)} & \dots & \mathbf{B}^{(j_{\max}-1)} & \mathbf{B}^{(j_{\max})} \\ \mathbf{I} & \mathbf{0} & \dots & \mathbf{0} & \mathbf{0} \\ \mathbf{0} & \mathbf{I} & \dots & \mathbf{0} & \mathbf{0} \\ \vdots & \vdots & \ddots & \vdots & \vdots \\ \mathbf{0} & \mathbf{0} & \dots & \mathbf{I} & \mathbf{0} \end{bmatrix} \begin{Bmatrix} \mathbf{U}^{(i)} \\ \mathbf{U}^{(i-1)} \\ \mathbf{U}^{(i-2)} \\ \vdots \\ \mathbf{U}^{(i-j_{\max}+2)} \\ \mathbf{U}^{(i-j_{\max}+1)} \end{Bmatrix}. \tag{123}$$

In this system, $\mathbf{B}^{(j)} = -[\mathbf{Z}^{(0)}]^{-1}[\mathbf{Z}^{(j)}]$, where $[\mathbf{Z}^{(j)}]$ is the appropriate matrix describing the interactions between radiation from a source j time steps ago. For instance, $[\mathbf{Z}^{(j)}]$ should be taken as one of the entire block matrices defined in (101) to analyze the stability of the D-APIE. Additionally, $\mathbf{U}^{(i)}$ is a column vector that contains the basis expansion coefficients for time step i. Finally, $\mathbf{I}$ is an identity matrix and $\mathbf{0}$ is a matrix entirely filled with zeros. It should be noted that (123) is not valid for analyzing the stability of the APIE. The presence of the recursive computation must also be accounted for to properly describe the MOT process for that case. More details on the needed modifications can be found in [25].

Clearly, once the MOT matrices have been calculated, the matrix in (123), termed the companion matrix, can be as well. The eigenvalues of the companion matrix may then be calculated to determine the stability of the method. If any eigenvalue is located outside the unit circle on the complex plane, the system is considered unstable. This is because this situation represents the ability for the system to continually increase the magnitude of the sources on the scattering object in the absence of any additional external excitation. Note that in addition to the eigenvalue stability analysis, we also allowed our codes to run for a large number of time steps after the excitation left the problem. This typically corresponded to somewhere between a few hundred to a few thousand transits of the geometry, with no indication of stability issues seen for the stable formulations.

5.1. Original A-Φ Formulation Results

The first numerical results that are presented are used to verify the claims made about the inherent instability of the original $\mathbf{A}$-Φ formulation discussed in Sections 3.1 and 3.5 for any basis and testing functions when using a MOT discretization scheme. Following these discussions, it was stated that since the equations utilize different temporal testing Sobolev spaces they cannot be discretized in a consistent manner using the MOT discretization method. From a simpler physical viewpoint, the two equations being used should exhibit a temporal balance for a MOT discretization to be stable. This necessary balance is missing in the original $\mathbf{A}$-Φ formulation, which is mathematically seen through the different temporal testing Sobolev spaces for the two equations. As a result, they will be extremely prone to instability if a MOT discretization is used.

Since no correct choice of MOT temporal basis functions exists for these equations, a quadratic B-spline basis function is used for both $\mathbf{J}$ and Σ to illustrate the instability. This is selected so that (93) is appropriately discretized and that the two temporal derivatives on Σ can be easily computed. The spatial discretization is also performed appropriately for both equations according to the variational formulation. This uses RWG functions for $\mathbf{J}$ and pulse functions for Σ, with (92) tested with RWG functions and (93) tested with pulse functions.

Despite the largely compliant discretization, results are still unstable, with two simulations presented to illustrate this. The first simulation uses a center frequency of 1 MHz, a bandwidth of 500 kHz, and a time step of 33.3 ns. The second simulation uses a center frequency of 80 MHz, a bandwidth of 20 MHz, and a time step of 0.5 ns. The results of the eigenvalue stability analysis for both simulations are shown in Fig. 2, which clearly shows the instability for both cases. Further, it is seen that the instability becomes substantially greater as the center frequency is increased.

As a comparison, MOT simulations were also performed for the 80 MHz center frequency simulation using traditional TDIE methods (e.g., the TD-EFIE, TD-MFIE, and TD-CFIE). The spatial discretization used RWG functions for both basis and testing functions, while the temporal discretization used a triangle function as basis to conform to the correct Sobolev space for the problems [27]. Although not shown here for brevity, these simulations were all

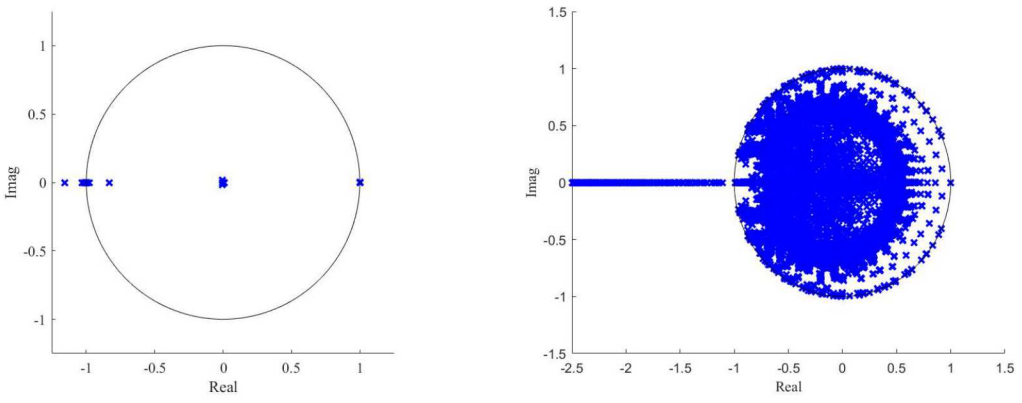

Fig. 2: Eigenvalues from the stability analysis for the original **A**-Φ formulation with center frequencies of (a) 1 MHz and (b) 80 MHz.

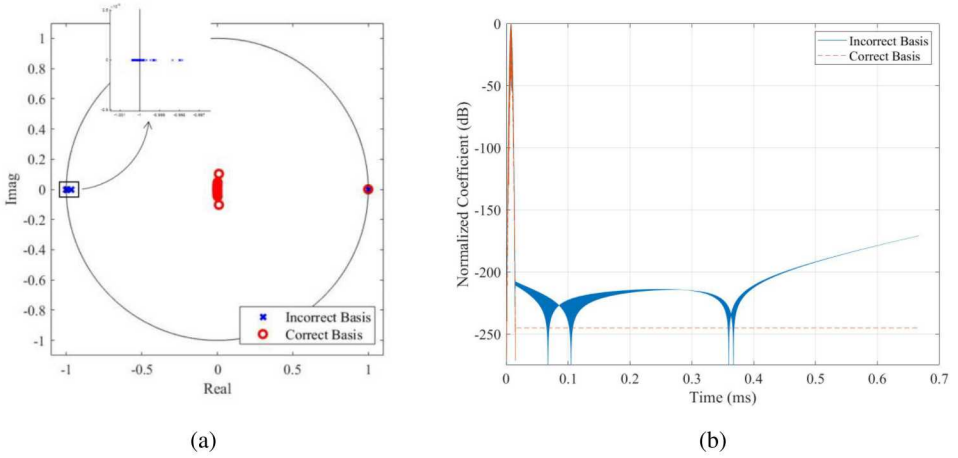

Fig. 3: Comparison of results for the D-APIE when incorrect and correct basis functions are used, (a) eigenvalues and (b) basis coefficients.

stable, and produced accurate results. Since it is desired to use the **A**-Φ formulation for multiscale modeling, it must be able to produce similar results at middle frequencies compared to traditional approaches. The substantial instability of the original **A**-Φ formulation does not meet this goal, necessitating the developments of this work.

5.2. D-APIE Results

The next claims that are verified are related to the D-APIE. In particular, it was claimed that using a temporal basis function from a subspace of the correct Sobolev space would lead to instability. This is demonstrated by using a quadratic B-spline function as the temporal basis function for **J** and Π. The same simulation parameters for the 1 MHz center frequency simulation are used again, with the results shown in Fig. 3. From the inset in the figure, a number of eigenvalues near $(-1,0i)$ are seen to lie outside of the unit circle. As a result, the system is unstable; however, it is seen that by using a set of equations that can be discretized consistently the stability of the method is greatly improved over the original **A**-Φ formulation discussed in the previous section. To further demonstrate the instability, the coefficients from one of the basis functions are also plotted in Fig. 3. The onset of the classic "late-time" instability is seen, verifying the claim that utilizing a basis function from a subspace of the correct Sobolev space can lead to an unstable system. It should also be noted that as the center frequency is increased, this method becomes increasingly unstable with eigenvalues moving further outside the unit circle. This results in the onset of instability occurring at increasingly earlier time steps in the simulation. As a result, this is not a robust enough discretization approach to be used in practice.

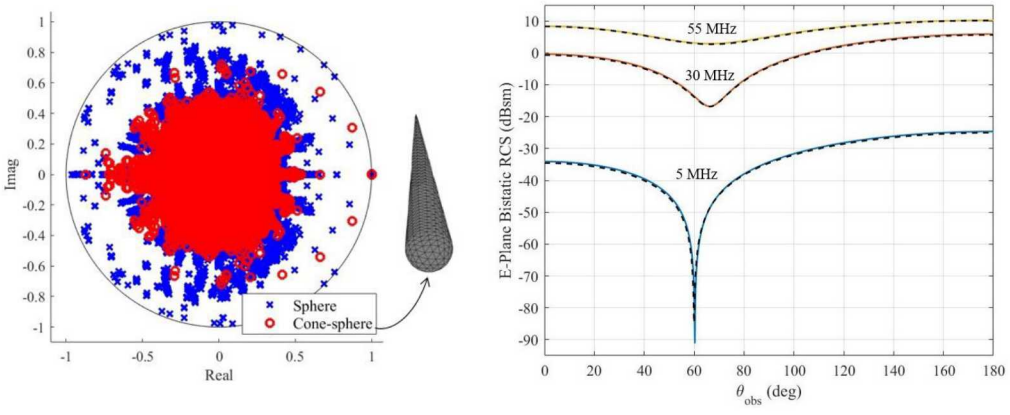

(a) (b)

Fig. 4: Results for the D-APIE when correct basis functions are used. The solid lines are analytical results while the dashed lines are numerical results. The RCS is shown at 5, 30, and 55 MHz. (a) Eigenvalue stability analysis and (b) RCS.

To demonstrate that this set of equations can be stably discretized, two examples are presented that follow the variational formulation in Section 3.3 and corresponding discretization outlined in Section 4.4. As was discussed, these equations can be discretized using the traditional MOT procedure if a triangular temporal basis function is used. This was done for the 1 meter radius sphere with a center frequency of 30 MHz, a bandwidth of 29 MHz, and a time step of 0.847 ns. Additionally, a simulation was also performed for a more complicated target, a cone-sphere, defined by the body-of-revolution line

$$\rho(z) = \begin{cases} 1.7429(z + 47.642), & \text{for } -47.642 < z < 0 \\ 5.894\sqrt{1 - \left(\dfrac{z - 0.718}{5.894}\right)^2}, & \text{for } 0 < z < 6.612, \end{cases} \tag{124}$$

where all dimensions are in inches. An image of the cone-sphere is shown in Fig. 4(a). The cone-sphere simulation was performed with a center frequency of 50 MHz, a bandwidth of 40 MHz, and a time step of 0.556 ns.

The results of the eigenvalue stability analysis for both simulations are shown in Fig. 4, where it is seen that all eigenvalues lie on or inside the unit circle denoting a stable system in practice. To demonstrate the accuracy of the method, the bistatic radar cross section (RCS) was calculated for the sphere simulation at 5, 30, and 55 MHz from the single simulation. All of these results are shown in Fig. 4. As anticipated, good accuracy is achieved over the entire bandwidth of the incident pulse.

5.3. APIE Results

The final set of claims of stability made throughout this work that needs to be verified are in reference to the APIE. One of the major claims was that using a temporal testing function from a subspace of the correct temporal Sobolev space would lead to instability. This is demonstrated by performing a simulation with the APIE using a triangular temporal basis function and a Dirac delta function for temporal testing. By recalling the discussion in Section 4.2, it is seen that this corresponds to using a temporal basis function from the correct space, but a temporal testing function from a subspace of the correct space. The simulation is performed at a center frequency of 30 MHz, a bandwidth of 29 MHz, and a time step of 0.847 ns. The results of the stability analysis are shown in Fig 5. It is seen that a large number of eigenvalues are located substantially outside of the unit circle, demonstrating the significant instability of the approach.

The next set of results demonstrates a stable discretization of the APIE system. In particular, the implementation discussed in Section 4.2 and equations presented in Section 4.5 are used. This utilized a pulse function as the temporal basis function in an otherwise standard MOT discretization. The first simulation is performed for the 1 meter radius sphere with a center frequency of 40 MHz, a bandwidth of 40 MHz, and a time step of 0.3125 ns. The second

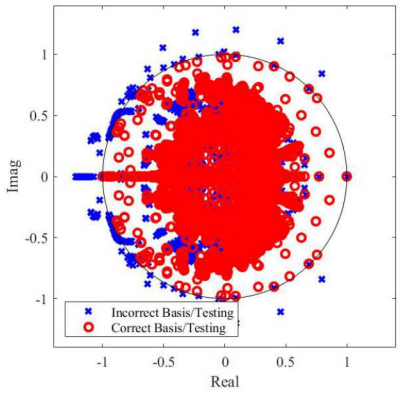

Fig. 5: Comparison of results of the eigenvalue stability analysis for the APIE when incorrect and correct testing functions are used.

simulation used a double ogive shape, which is defined by the body-of-revolution line

$$\rho(z) = \begin{cases} \dfrac{5f(z)}{1-\cos(46.4^\circ)}, & \text{for } -12.5 < z < 0 \\ \dfrac{5g(z)}{1-\cos(22.62^\circ)}, & \text{for } 0 < z < 25, \end{cases} \tag{125}$$

where

$$f(z) = \sqrt{1-\left(\frac{z}{12.5}\right)^2 \sin^2(46.6^\circ)} - \cos(46.6^\circ), \tag{126}$$

$$g(z) = \sqrt{1-\left(\frac{z}{25}\right)^2 \sin^2(22.62^\circ)} - \cos(22.62^\circ), \tag{127}$$

and all dimensions are in inches. An image of the double ogive is shown in Fig. 6(a). The double ogive was simulated with a center frequency of 50 MHz, a bandwidth of 40 MHz, and a time step of 0.556 ns.

The results of the stability analysis are shown in Fig 6. All of the eigenvalues lie on or inside of the unit circle, demonstrating the stability of the discretization in practice. To verify the accuracy of the method, the RCS of the sphere was calculated at 10, 40, and 70 MHz. From this it is seen that good results are achieved over the bandwidth of the incident pulse.

5.4. Stability Stress Test

Before moving on to demonstrating the low frequency performance of these methods, we present a few final stability stress tests for the methods when correct basis and testing functions are used in the discretization. It is generally considered that thin structures pose an especially challenging geometry to MOT TDIE solvers. In accordance with this, we have selected as a stressing geometry to take the double ogive geometry defined in the previous section and reduce its thickness by a factor of 10. The resulting geometry is shown in the inset of Figure 7(b).

Two simulations are performed for this geometry. The first uses a center frequency of 50 MHz, a bandwidth of 40 MHz, and a time step of 0.556 ns. The second simulation increases the frequency to 100 MHz, with a bandwidth of 80 MHz and time step of 0.278 ns. The results are shown in Figure 7, where it is seen that every simulation is stable. Note that no eigenvalues were calculated for the 100 MHz simulation for the APIE. This is due to the large size of the resulting matrix system that made it impractical. To demonstrate the stability for this case, the solved for coefficients of one spatial basis function are plotted in Figure 7(b) for 100,000 time steps. This corresponds to over 7,500 transits of the geometry, with no stability issues observed. The currents for the D-APIE simulation are also plotted for comparison.

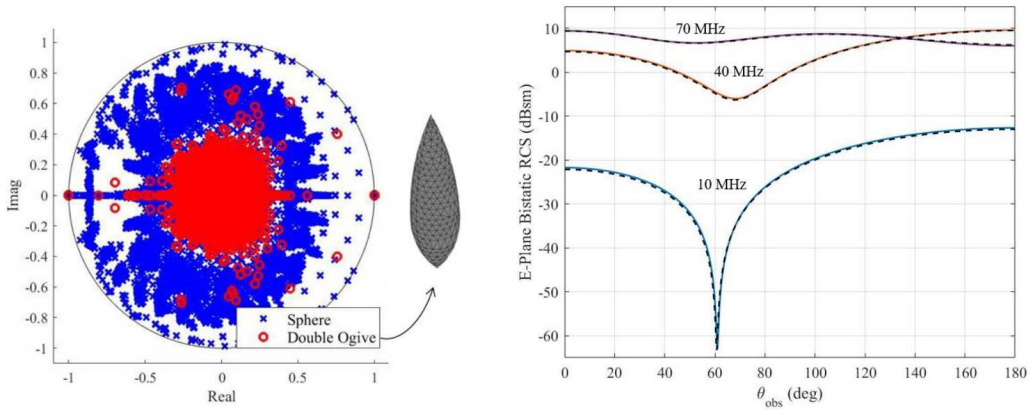

(a) (b)

Fig. 6: Results for the APIE when correct basis functions are used. The solid lines are analytical results while the dashed lines are numerical results. The RCS is shown at 10, 40, and 70 MHz. (a) Eigenvalue stability analysis and (b) RCS.

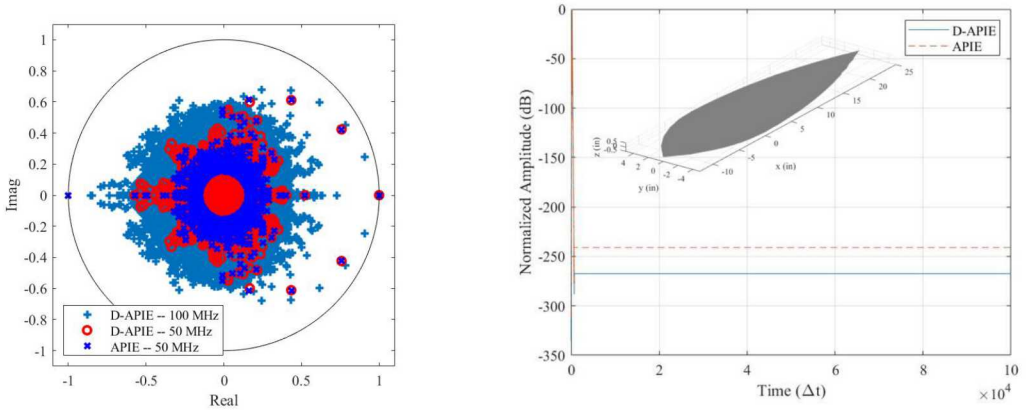

(a) (b)

Fig. 7: Stability stress test results for the 50 and 100 MHz simulations. (a) Eigenvalue stability analysis and (b) normalized coefficients for the APIE and D-APIE in the 100 MHz simulation and thin double ogive geometry.

5.5. Low Frequency Results

The previous sections demonstrated that by properly selecting the basis and testing functions according to the functional framework detailed in this work, stable results could be achieved. This is an important step towards demonstrating that the different APIEs are suitable for multiscale analysis. However, in addition to stability and accuracy at middle frequencies, the same must be achievable at low frequencies. As a result, a number of tests are performed in this section to demonstrate the stability and accuracy of the APIEs at low frequencies.

As an initial demonstration, the improvement of the APIEs over the traditional EFIE is shown when the EFIE is beginning to be affected by the well-known low frequency breakdown. The simulation is performed with a center frequency of 40 MHz, a bandwidth of 40 MHz, and a time step of 0.3125 ns. Simulations are performed with the APIE, D-APIE, and the EFIE. No modifications are performed to the EFIE to improve its low frequency performance. The RCS is plotted at 10 MHz in Fig. 8(a). It is seen that even at this frequency, the EFIE is already becoming inaccurate while the accuracy of both the APIE and D-APIE is good.

To further demonstrate the accuracy of the APIE and D-APIE at low frequencies a sequence of simulations with progressively lower center frequencies is performed. The error at the center frequency of each simulation is calculated

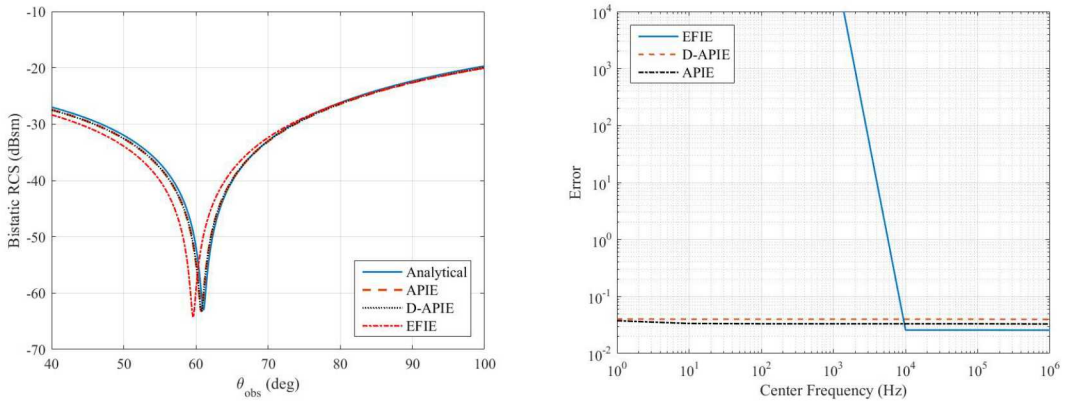

(a) (b)

Fig. 8: Results for the APIE, D-APIE, and EFIE at (a) 10 MHz and (b) over a sequence of simulations.

using

$$\text{Error} = \frac{\|\text{RCS}_{\text{TDIE}} - \text{RCS}_{\text{Mie}}\|}{\|\text{RCS}_{\text{Mie}}\|}, \tag{128}$$

where $\|\cdot\|$ is the ℓ_2 norm, RCS_{TDIE} is the RCS calculated using the specified TDIE, and RCS_{Mie} is the RCS calculated with the Mie series. To compute RCS_{TDIE}, the computed time domain current density is Fourier transformed to the frequency domain. The appropriate frequency domain current distribution is then used to compute the far-field RCS. The RCS_{Mie} results are computed directly in the frequency domain.

For all cases, the RCS used is the E-plane bistatic RCS over a range from 0 to 180° in 0.1° increments. The simulations cover center frequencies of 1 Hz to 1 MHz with the bandwidth set to half the center frequency. The oversampling factor s is set to 20 for all cases. The error is plotted in Fig. 8(b) which shows the steady accuracy of both the D-APIE and APIE. As anticipated, the EFIE (with no low frequency modifications made) eventually experiences a catastrophic low frequency breakdown resulting in an unstable solution. This highlights the strength of the **A**-Φ formulation TDIEs presented in this work. That is, no intricate modifications are needed to the equations or discretization approach to produce accurate results over a very wide range of frequencies.

6. Conclusion

This work presented the details of a rigorous functional framework that has found great use in analyzing TDIEs. It is anticipated that as the computational electromagnetics community continues to become more involved with applications in emerging areas of physics, this type of rigorous functional analysis will become more needed in the derivation of new integral equations. This was demonstrated by applying the functional framework discussed to derive a set of TDIEs based on the **A**-Φ formulation, which is expected to be well-suited to coupling into quantum physics calculations. Following this derivation, the necessary functional analysis was presented which demonstrates the stability of these **A**-Φ TDIEs. It was then discussed how information from the functional analysis could be used to devise MOT discretization approaches that would produce stable systems in practice. Numerical results were then presented that verified the different claims of stability or instability for systems made throughout this work. The results also demonstrated the superior performance of this formulation for analyzing systems at low frequencies, making these equations suitable for use in multiscale modeling.

The current **A**-Φ TDIEs discussed in this work are only applicable to analyzing perfect electric conducting objects. Future work will focus on extending this formulation to cover dielectric/penetrable objects, which are of far greater interest to many applications, e.g., in the area of quantum optics. Other practical considerations for this formulation also need to be investigated, such as the performance of preconditioners.

Acknowledgments

This work was supported by Sandia National Laboratories Critical Skills Master's Program and Tuition Assistance Program, AF Sub RRI PO0539, NSF ECCS 169195, Ansys Inc PO37497, the George and Ann Fisher Professorship at the University of Illinois at Urbana-Champaign, and the Distinguished Professorship Grant at Purdue University.

This paper describes objective technical results and analysis. Any subjective views or opinions that might be expressed in the paper do not necessarily represent the views of the U.S. Department of Energy or the United States Government.

Sandia National Laboratories is a multimission laboratory managed and operated by National Technology & Engineering Solutions of Sandia, LLC, a wholly owned subsidiary of Honeywell International Inc., for the U.S. Department of Energy's National Nuclear Security Administration under contract DE-NA0003525.

References

[1] W. C. Chew, Vector potential electromagnetics with generalized gauge for inhomogeneous media: Formulation, Progress In Electromagnetics Research 149 (2014) 69–84.
[2] W. C. Chew, A. Y. Liu, C. Salazar-Lazaro, W. E. I. Sha, Quantum electromagnetics: A new look–Part I, IEEE Journal on Multiscale and Multiphysics Computational Techniques 1 (2016) 73–84.
[3] M. Fox, Quantum Optics: An Introduction, volume 15, Oxford University Press, 2006.
[4] C. Cohen-Tannoudji, J. Dupont-Roc, G. Grynberg, Atom-Photon Interactions: Basic Processes and Applications, Wiley, 1992.
[5] A. W. Rodriguez, F. Capasso, S. G. Johnson, The Casimir effect in microstructured geometries, Nature Photonics 5 (2011) 211–221.
[6] A. P. McCauley, A. W. Rodriguez, J. D. Joannopoulos, S. G. Johnson, Casimir forces in the time domain: Applications, Physical Review A 81 (2010) 012119.
[7] C. J. Ryu, A. Y. Liu, W. E. I. Sha, W. C. Chew, Finite-difference time-domain simulation of the Maxwell–Schrödinger system, IEEE Journal on Multiscale and Multiphysics Computational Techniques 1 (2016) 40–47.
[8] J. L. Xiong, M. S. Tong, P. Atkins, W. C. Chew, Efficient evaluation of Casimir force in arbitrary three-dimensional geometries by integral equation methods, Physics Letters A 374 (2010) 2517–2520.
[9] A. Y. Liu, W. C. Chew, Dressed atom fields and dressed states in waveguide quantum electrodynamics, IEEE Journal on Multiscale and Multiphysics Computational Techniques 2 (2017) 58–65.
[10] P.-F. Qiao, W. E. I. Sha, W. C. H. Choy, W. C. Chew, Systematic study of spontaneous emission in a two-dimensional arbitrary inhomogeneous environment, Physical Review A 83 (2011) 043824.
[11] N.-W. Chen, K. Aygun, E. Michielssen, Integral-equation-based analysis of transient scattering and radiation from conducting bodies at very low frequencies, IEE Proceedings-Microwaves, Antennas and Propagation 148 (2001) 381–387.
[12] K. Cools, F. P. Andriulli, F. Olyslager, E. Michielssen, Time domain Calderón identities and their application to the integral equation analysis of scattering by PEC objects Part I: Preconditioning, IEEE Transactions on Antennas and Propagation 57 (2009) 2352–2364.
[13] F. P. Andriulli, A. Tabacco, G. Vecchi, Solving the EFIE at low frequencies with a conditioning that grows only logarithmically with the number of unknowns, IEEE Transactions on Antennas and Propagation 58 (2010) 1614–1624.
[14] Y.-L. Li, S. Sun, Q. I. Dai, W. C. Chew, Finite element implementation of the generalized-Lorenz gauged A-Φ formulation for low-frequency circuit modeling, IEEE Transactions on Antennas and Propagation 64 (2016) 4355–4364.
[15] Q. S. Liu, S. Sun, W. C. Chew, A potential based integral equation method for low-frequency electromagnetic problems, IEEE Transactions on Antennas and Propagation 66 (2018) 1413–1426.
[16] T. E. Roth, W. C. Chew, Development of stable A-Φ time domain integral equations for multiscale electromagnetics (accepted for publication, 2018).
[17] B. Shanker, A. A. Ergin, M. Lu, E. Michielssen, Fast analysis of transient electromagnetic scattering phenomena using the multilevel plane wave time domain algorithm, IEEE Transactions on Antennas and Propagation 51 (2003) 628–641.
[18] A. E. Yilmaz, J.-M. Jin, E. Michielssen, Time domain adaptive integral method for surface integral equations, IEEE Transactions on Antennas and Propagation 52 (2004) 2692–2708.
[19] T. Ha-Duong, On retarded potential boundary integral equations and their discretisation, in: Topics in Computational Wave Propagation, Springer, 2003, pp. 301–336.
[20] P. J. Davies, D. B. Duncan, Averaging techniques for time-marching schemes for retarded potential integral equations, Applied Numerical Mathematics 23 (1997) 291–310.
[21] D. S. Weile, G. Pisharody, N.-W. Chen, B. Shanker, E. Michielssen, A novel scheme for the solution of the time-domain integral equations of electromagnetics, IEEE Transactions on Antennas and Propagation 52 (2004) 283–295.
[22] X. Wang, R. A. Wildman, D. S. Weile, P. Monk, A finite difference delay modeling approach to the discretization of the time domain integral equations of electromagnetics, IEEE Transactions on Antennas and Propagation 56 (2008) 2442–2452.
[23] B. Shanker, M. Lu, J. Yuan, E. Michielssen, Time domain integral equation analysis of scattering from composite bodies via exact evaluation of radiation fields, IEEE Transactions on Antennas and Propagation 57 (2009) 1506–1520.
[24] H. A. Ülkü, A. A. Ergin, Application of analytical retarded-time potential expressions to the solution of time domain integral equations, IEEE Transactions on Antennas and Propagation 59 (2011) 4123–4131.
[25] A. J. Pray, N. V. Nair, B. Shanker, Stability properties of the time domain electric field integral equation using a separable approximation for the convolution with the retarded potential, IEEE Transactions on Antennas and Propagation 60 (2012) 3772–3781.
[26] K. Cools, F. P. Andriulli, E. Michielssen, A Calderón multiplicative preconditioner for the PMCHWT integral equation, IEEE Transactions on Antennas and Propagation 59 (2011) 4579–4587.

[27] E. van't Wout, D. R. van der Heul, H. van der Ven, C. Vuik, Stability analysis of the marching-on-in-time boundary element method for electromagnetics, Journal of Computational and Applied Mathematics 294 (2016) 358–371.
[28] I. Terrasse, Résolution mathématique et numérique des équations de Maxwell instationnaires par une méthode de potentiels retardés, Ph.D. thesis, 1993.
[29] A. Bachelot, L. Bounhoure, A. Pujols, Couplage éléments finis-potentiels retardés pour la diffraction électromagnétique par un obstacle hétérogène, Numerische Mathematik 89 (2001) 257–306.
[30] T. Ha-Duong, B. Ludwig, I. Terrasse, A Galerkin BEM for transient acoustic scattering by an absorbing obstacle, International Journal for Numerical Methods in Engineering 57 (2003) 1845–1882.
[31] E. Van't Wout, Stability, accuracy, and robustness of the time domain integral equation method for radar scattering analysis, Ph.D. thesis, 2013.
[32] A. Bamberger, T. Ha-Duong, J. C. Nédélec, Formulation variationnelle espace-temps pour le calcul par potentiel retardé de la diffraction d'une onde acoustique (I), Mathematical methods in the applied sciences 8 (1986) 405–435.
[33] A. Pujols, Equations intégrales espace-temps pour le système de Maxwell application au calcul de la surface equivalente radar, Ph.D. thesis, 1991.
[34] M. E. Hassell, T. Qiu, T. Sanchez-Vizuet, F.-J. Sayas, A new and improved analysis of the time domain boundary integral operators for the acoustic wave equation, Journal of Integral Equations and Applications 29 (2017) 107–136.
[35] G. C. Hsiao, R. E. Kleinman, Mathematical foundations for error estimation in numerical solutions of integral equations in electromagnetics, IEEE Transactions on Antennas and Propagation 45 (1997) 316–328.
[36] S. Rao, D. Wilton, A. Glisson, Electromagnetic scattering by surfaces of arbitrary shape, IEEE Transactions on Antennas and Propagation 30 (1982) 409–418.
[37] W. C. Chew, Waves and Fields in Inhomogeneous Media, IEEE Press, 1995.
[38] A. Bachelot, V. Lange, Time dependent integral method for Maxwell's system, Mathematical and Numerical Aspects of Wave Propagation (1995) 151–159.
[39] J.-C. Nédélec, Acoustic and Electromagnetic Equations: Integral Representations for Harmonic Problems, volume 144, Springer Science & Business Media, 2001.
[40] J. A. Stratton, Electromagnetic Theory, John Wiley & Sons, 2007.
[41] M. Benzi, G. H. Golub, J. Liesen, Numerical solution of saddle point problems, Acta Numerica 14 (2005) 1–137.
[42] M. M. Jia, Y. W. Zhao, S. Sun, Analysis and stabilization of the low-frequency time-domain augmented EFIE, IEEE Antennas and Wireless Propagation Letters 15 (2016) 1751–1754.
[43] V. H. Rumsey, Reaction concept in electromagnetic theory, Physical Review 94 (1954) 1483.
[44] Q. I. Dai, W. C. Chew, L. J. Jiang, Y. Wu, Differential-forms-motivated discretizations of electromagnetic differential and integral equations, IEEE Antennas and Wireless Propagation Letters 13 (2014) 1223–1226.
[45] A. J. Pray, Y. Beghein, N. V. Nair, K. Cools, H. Bağcı, B. Shanker, A higher order space-time Galerkin scheme for time domain integral equations, IEEE Transactions on Antennas and Propagation 62 (2014) 6183–6191.
[46] Y. Beghein, K. Cools, H. Bagci, D. De Zutter, A space-time mixed Galerkin marching-on-in-time scheme for the time-domain combined field integral equation, IEEE Transactions on Antennas and Propagation 61 (2013) 1228–1238.
[47] E. van't Wout, D. R. van der Heul, H. van der Ven, C. Vuik, The influence of the exact evaluation of radiation fields in finite precision arithmetic on the stability of the time domain integral equation method, IEEE Transactions on Antennas and Propagation 61 (2013) 6064–6074.
[48] P. Yla-Oijalä, M. Taskinen, Calculation of CFIE impedance matrix elements with RWG and n×RWG functions, IEEE Transactions on Antennas and Propagation 51 (2003) 1837–1846.
[49] Z.-G. Qian, W. C. Chew, Fast full-wave surface integral equation solver for multiscale structure modeling, IEEE Transactions on Antennas and Propagation 57 (2009) 3594–3601.
[50] X. Tian, G. Xiao, Time-domain augmented electric field integral equation for a robust marching on in time solver, IET Microwaves, Antennas & Propagation 8 (2014) 688–694.
[51] S. Walker, M. Bluck, I. Chatzis, The stability of integral equation time-domain scattering computations for three-dimensional scattering; similarities and differences between electrodynamic and elastodynamic computations, International Journal of Numerical Modelling: Electronic Networks, Devices and Fields 15 (2002) 459–474.